POLITECNICO
MILANO 1863

SCUOLA DI INGEGNERIA INDUSTRIALE
E DELL'INFORMAZIONE

Molecular Separation Using $M_{12}L_8$ Nanocages And Tris-Pyridyl Benzene Ligand Functionalization

MASTER OF SCIENCE IN CHEMICAL ENGINEERING

Author: **Alessandro Zanotti**

Student ID: 996932
Advisor: Prof. Javier Marti-Rujas
Co-advisor: Dr. Stefano Elli
Academic Year: 2022-23

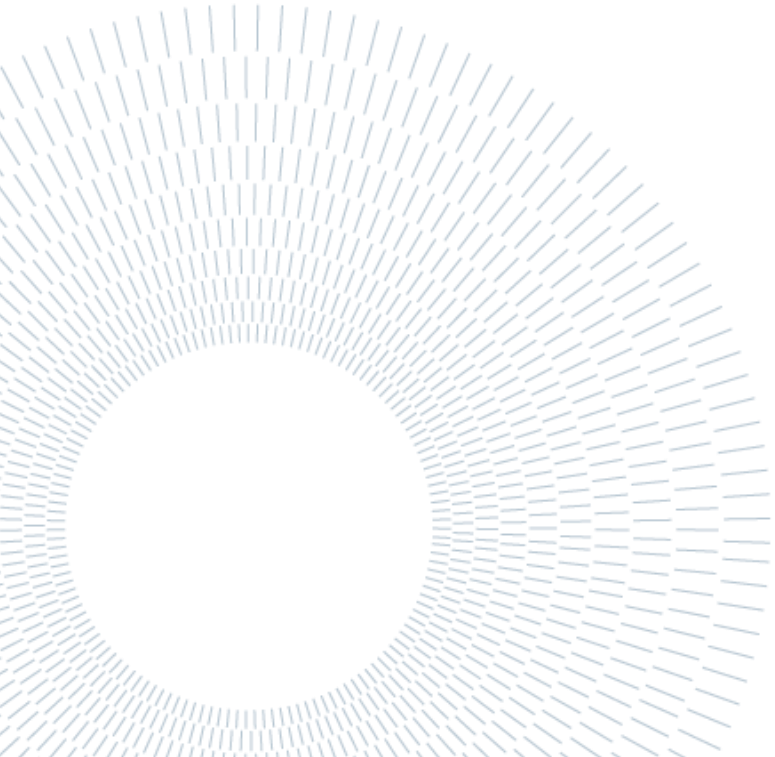

"The automobile engine will come, and then
I will consider my life's work complete."

Rudolf Diesel, 1858-1913

Abstract

Poly-[*n*]-catenanes self-assembled of metal organic cages (MOCs), which are classified as mechanically interlocked materials (MIMs), are receiving much attention because of their fascinating structures and because of their potential applications as functional materials. These architectures spontaneously form by the self-assembly of metal ions and organic ligands and in many cases remain stable in the solid-state. Properties which emerge from these singular topologies pave the way for a vast array of potential applications in materials science, engineering, etc. Following the previous work, my last year activity focused on the influence that the exo-tridentate ligands (*tris*-pyridyl benzenes, TPBs) have in the formation of $M_{12}L_8$ nanocages, on the one hand, and on their host-guest chemistry once formed, on the other hand.

In particular, the molecular recognition ability of ZnI_2-TPB poly-[*n*]-catenanes are investigated, both in crystal and powder form. $M_{12}L_8$ nanocages single crystals are produced via three-layer method with para-xylene as templating agent. After its characterization through Single Crystal-X Ray Diffraction (SC-XRD), the confirmed molecular recognition through π–π binding sites let them be tested for gas-solid reactions (*i.e.*, single-crystal-to-single-crystal guest exchange), which indeed occurs successfully. Then, consecutive gas-solid guest exchanges with different aromatic vapours were tested, checking whether a preferential molecular recognition arises as confirmed by SC-XRD and Density Functional Theory (DFT).

Afterwards, attention switched to microcrystalline (i.e., powder) $M_{12}L_8$ nanocages, wherein the same results are tested for liquid-powder reactions. Actually, beyond the different behaviour found, separation of isomers of petrochemical species (above all, xylenes) and selective adsorption of pollutant species (starting from nitrobenzene) were tested. Different inclusions and consecutive exchanges highlight whether a templating effect and an uptake preference arises which were studied by powder XRD and solution ^{1}H-NMR techniques.

Parallelly, on the line of previously acquired knowledge about ligand functionalization (*i.e.*, addition of methyl groups), my work consisted in the yield improvement and minimization of solvent used in the synthesis. A change in the synthetic conditions by changing both the catalyst and the quantities, were carried out. Also, the work-up process was modified, leading to a significant enhance of yield and solvent minimization. Thereafter, the application of the methylated TPB ligand in the catenane's formation (i.e., $M_{12}L_8$ assembly) was investigated, finding out significant changes. Indeed, small methylation makes planar coordination networks more stable than interlocked cages which have completely different structural and host-guest properties.

Key-words: MIMs – MOCs - poly-[n]-catenane - SC-XRD - molecular recognition - isomer separation - ligand synthesis - ligand functionalization

Sommario

I poli-[n]-catenani, auto-assemblati in gabbie metallorganiche (MOC), classificati come molecole meccanicamente interconnesse (MIM), stanno ricevendo molta attenzione per le loro affascinanti strutture e per le loro potenziali applicazioni come materiali funzionalizzabili. Queste architetture si formano spontaneamente dall'autoassemblaggio di ioni metallici e ligandi organici e in molti casi rimangono stabili allo stato solido. Le proprietà che emergono da queste singolari topologie aprono la strada a una vasta gamma di potenziali applicazioni nella scienza dei materiali, nell'ingegneria, ecc. Seguendo il lavoro precedente, la mia attività dell'ultimo anno si è concentrata sull'influenza che i ligandi eso-tridentati (tris-piridilbenzeni, TPB) hanno nella formazione delle nanocaviglie $M_{12}L_8$, da un lato, e sulla loro host-guest chemistry una volta formate, dall'altro.

In particolare, è stata studiata la capacità di riconoscimento molecolare dei poli-[*n*]-catenani di ZnI_2-TPB, sia in forma di cristallo che di polvere. I monocristalli di catenani $M_{12}L_8$ sono stati prodotti con il metodo a tre strati con para-xilene come agente templante. Dopo la caratterizzazione mediante diffrazione a raggi-X di cristalli singoli (SC-XRD), il riconoscimento molecolare è confermato attraverso i siti di legame di π–π ha permesso di testare le reazioni gas-solido (cioè il guest echange single-crystal-to-single-crystal), che si è verificato con successo. In seguito, sono stati testati scambi consecutivi di guest gas-solido con diversi vapori di aromatici, come confermato dalla SC-XRD e dalla Density Functional Theory (DFT).

In seguito, l'attenzione si è spostata su microcristalli (cioè, polvere) $M_{12}L_8$, dove sono stati verificati gli stessi risultati per le reazioni solido-liquido. In realtà, al di là del diverso comportamento riscontrato, sono stati testati la separazione di isomeri di specie petrolchimiche (soprattutto xileni) e l'adsorbimento selettivo di specie inquinanti (a partire dal nitrobenzene). Le diverse inclusioni e gli scambi consecutivi evidenziano la presenza di un effetto di templatura e di una preferenza di assorbimento, studiati con tecniche di XRD della polvere e di ^{1}H-NMR in soluzione. Parallelamente, sulla linea delle conoscenze precedentemente acquisite sulla funzionalizzazione dei ligandi (cioè l'aggiunta di gruppi metilici), il mio lavoro è consistito nel miglioramento della resa e nella minimizzazione del solvente utilizzato nella sintesi. Sono state modificate le condizioni di sintesi cambiando sia il catalizzatore che le quantità. Inoltre, è stato modificato il processo di lavorazione. Successivamente, è stata studiata l'applicazione del ligando TPB metilato nella formazione del catenano (cioè l'assemblaggio $M_{12}L_8$), riscontrando cambiamenti significativi. Infatti, una piccola metilazione rende le reti di coordinazione planari più stabili, che hanno proprietà strutturali diverse.

Parole chiave: poly-[*n*]-catenane - interlocked nanocages – riconoscimento molecolare - separazione di isomeri - sintesi di ligandi – funzionalizzazione di ligandi

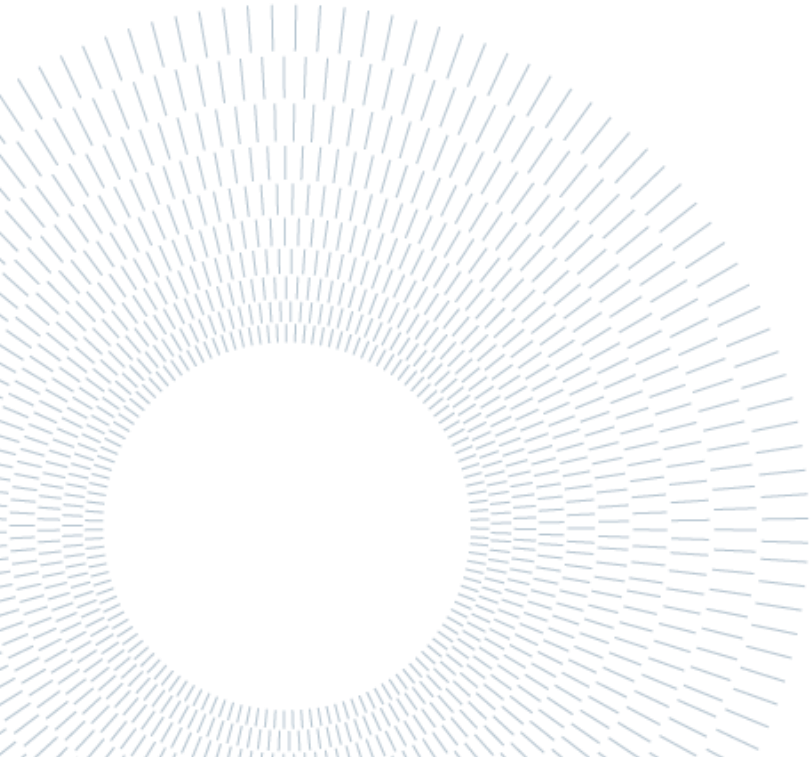

Contents

1 INTRODUCTION. THEORETICAL BACKGROUND

1.1. Catenanes made of Metal-Organic Cages

Given the primary focus of this work on poly-[*n*]-catenanes, with a specific emphasis on Catenanes made of MOCs, it would be beneficial to consider some cornerstones.

1.1.1. Topological perspective on supramolecular chemistry

Supramolecular chemistry accounts for the self-assembly of molecular architectures (through hydrogen bonding, π–π stacking interactions etc), which are stable in many cases. In this context, a topological perspective is interesting to be considered.
Since this work deals with nanocages, catenanes and coordination polymers, and their properties lie also in their geometry (just consider the *guest uptake*), it is worthy to think about later mentioned nanocages as 0-dimensional (0D) entities: they are well-known since 1995 [1] and exhibit thermodynamic stability and guest uptake. In *Results and Discussion* icosahedral nanocages (with internal volume per nanocage of ca. 2600-2700 $Å^3$ [2–4]) will be investigated.

Furthermore, more recent studies have identified how an interlocked set of nanocages leads to 1D poly-[*n*]-catenanes whose wide voids of each cage are compensated by sliding and interlocking of the chain (this enhance guest uptake and separation properties) [4,5].

Finally, if no interlocking occurs (see *Results and Discussion: Ligand functionalization*), the most stable structure is a 2D coordination network, wherein many properties are lost. A schematic representation is shown below (***Figure 1***).

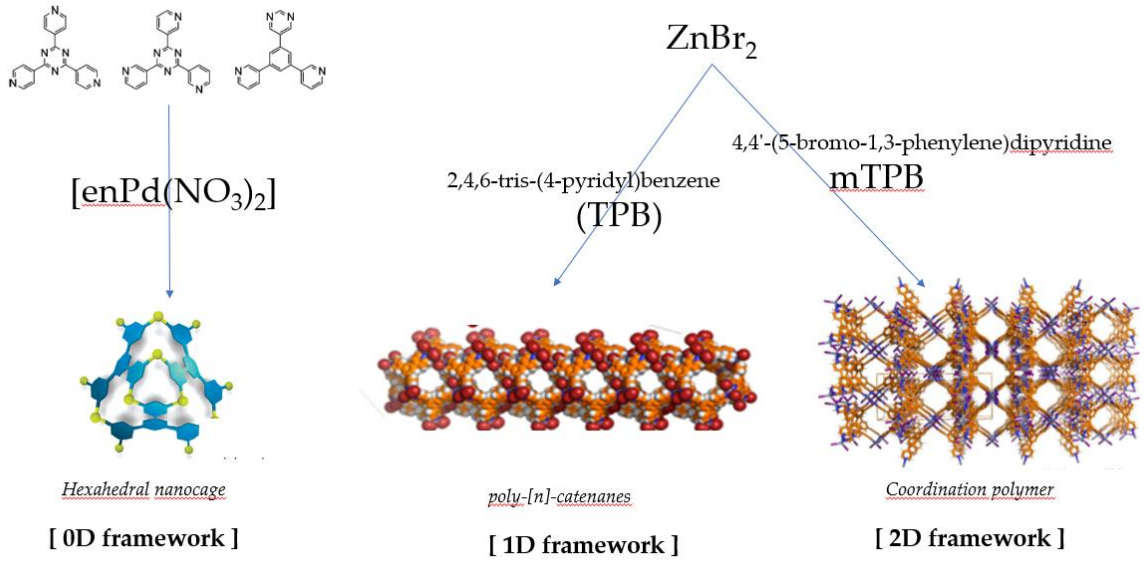

Figure 1 *Topological perspective on supramolecular structures*

1.1.2. Catenanes and polycatenanes

In material science and supramolecular chemistry, Catenanes and polycatenanes are molecular structures that offer opportunities for exploring new forms of molecular assembly and design of functional materials: especially from an engineering point of view, their potential applications make them a rich area of research and innovation [6–10]. These structures are metal-organic frameworks materials which are mechanically interlocked and are referred as mechanically interlocked materials (MIMs) and can be synthesized through *solid-state chemistry*, or in solution by *click chemistry* or *template-directed approach* [6–10]. Catenanes captivated the attention of researchers for over seven decades, with their first theoretical conception traced back to the works of Frisch et al. in 1953 and Patat and Derst in 1959 [11], although their synthesis remained unrealized at that time.

Definition and contextualization

Catenanes (or, better, Poly-[n]-catenanes) are defined by IUPAC as: "*Hydrocarbons having two or more rings connected in the manner of links of a chain, without a covalent bond. More generally, the class catena compounds embraces functional derivatives and hetero analogues*"[3,4]. They are type of mechanically interlocked molecule that consists of two or more macrocycles (tipically, ligands) that are linked together by a mechanical bond. The macrocycles can move relative to each other, but they cannot be separated without breaking the bond. Their stability relies on their topological arrangement,

making them remarkably stable: this makes them even more attractive for engineering applications (such as molecular recognition [3,12,13], gas storage [14–17], sensing applications and so on).

Properties and key features

Due to their intricate mechanical interlocking of rings, Catenanes offer an array of properties which peculiarities arise from the absence of covalent bonds between the rings, resulting in a topology, mechanics, scaling behaviour, rheology and (especially in our case) host-guest chemistry. One of the hallmarks of catenanes lies, indeed, in their **topological resilience**. Unlike traditional polymers, where covalent bonds govern behaviour, catenanes derive their structural integrity from the non-covalent mechanical linkages between rings . This arrangement results in remarkable flexibility and freedom of motion among the rings, allowing them to rotate, elongate, collapse, and even twist relative to each other [18,19]. The resultant mechanical bond opens a new dimension of behaviour that is inaccessible to standard polymers [4,7,18] Moreover, the **scaling behaviour** of individual rings within catenanes exhibits intriguing deviations from ordinary polymer scaling: in solution, molecular simulations reveal that catenated rings display scaling behaviour similar to linear and cyclic polymers arising from the mechanical bond [20]. Swelling ratios increase as the number of catenating rings rises, providing insights into the interplay between mechanical bonds and solvent interactions. Additionally, linear poly-[n]-catenanes, in particular, exhibit scaling properties akin to ordinary linear polymers, though their dimensions are inherently influenced by the mechanical interlocking. **Elasticity and mechanical properties** of catenanes emerge as a fascinating interplay between topological entanglements and elasticity. While linear poly-[n]-catenanes resemble traditional polymers in their Hookean-like elasticity at small deformations, their large deformation behaviour is distinctly non-Hookean, with a force-to-deformation relationship deviating from the typical quadratic scaling [21]. Interestingly, Olympic gels composed of densely interlocked rings showcase exceptional softness and extensibility, highlighting the role of sliding interlocked components in dictating macroscopic mechanical properties [22]. Furthermore, Catenanes introduce a paradigm shift in **rheology** and dynamic properties – the dynamics of catenanes in solution and the melt reveal intricate kinetic behaviours that distinguish them from their linear and cyclic counterparts. Molecular simulations illustrate that the mechanical bond imposes a slowdown in ring relaxation dynamics at the scale of the overall ring. Last but not least, poly-[n]-catenanes exhibit distinct dynamics, showcasing a separation between ring-like and chain-like motions, leading to sub-diffusive regimes in monomer displacement. [21]

Engineering applications

Notwithstanding the applications of MOFs and Catenanes, in general, and Catenanes made of MOCs, in particular, will be widely discussed in a dedicated chapter, a brief summary is deemed useful. Essentially, applications take use of catenanes' interlocked design to create new functional materials.

The intricate entanglement of catenanes mimics biological systems' complexity. Responsive materials with catenanes whose shape change when stimulated exist. That is particularly useful for smart materials, drug delivery systems, and environmental-responsive self-healing materials. **Nanoscale electronics** – because of their rotation, elongation, and twisting properties – make them promising candidates for complex molecular machines. Researchers are investigating ways to use catenanes' interlocked structure to create state-changing molecular switches [23]. These switches could advance nanotechnology by making tiny sensors, actuators, and computing components. Dynamic catenanes are ideal for creating **stimuli-responsive materials** that adapt to their surroundings. Researchers can use catenanes to build polymer networks that change form, stiffness, or conductivity with temperature, pH, or light. Adaptable coatings and soft robotics may benefit from these materials. [24]

1.1.3. Metal-Organic Cages

Metal-Organic Cages (MOCs) are a class of porous materials that are composed of metal ions or clusters connected by organic ligands to form three-dimensional cage-like structures. These structures exhibit well-defined and tunable pores that can host guest molecules, making them of great interest in the field of material science and supramolecular chemistry.

Properties and peculiarities

Beyond their porous nature (in common with MOFs) and their guest uptake property (in common with catenanes), key features of MOCs are their **structure and assembly** (MOCs are assembled through coordination bonds between metal ions or clusters and organic ligands. The choice of metal ions, ligands, and their connectivity determines the overall structure of the cage.

State of art

Among the acknowledged MOCs, those built upon di- or trivalent metal cations linked by carboxylate ligands stand out as optimal candidates due to their exceptional robustness, porosity, and surface area [8]. Their ease of synthesis at ambient conditions or through solvothermal methods has prompted significant interest in enhancing the

repertoire of cage structures by employing diverse bridging ligands with varying coordination capacities and geometries. These structures lend themselves well to subsequent functionalization, paving the way for a multitude of potential applications. Notably, zirconium-based metal-organic cages (Zr-MOCs) represent a paradigmatic instance of carboxylate-based MOCs, showcasing remarkable chemical and thermal stability, as well as solubility that widens their prospects in solution-based applications [7]. Nevertheless, only a limited number of publications have explored Zr-MOCs. Discrete molecular assemblies exhibit distinct structural characteristics compared to extended networks, which arise from the connectivity of molecular building blocks dictating the resultant structure, whether it be an isolated MOC or an extended MOF network [7]. The assembly of MOCs into higher-order structures leads to multidimensional ensembles. In this scenario, MOCs act as supramolecular platforms that interconnect, yielding continuous structures with polyhedral vertices: these high-order superstructures can manifest as various soft materials, such as polymers, metallohydrogels, infinite chains, infinite polycatenanes, and so on [24]. Consequently, some published works have pursued this approach, often termed the "cage-to-framework" strategy, aimed at enriching the chemical library with novel structures primed for unprecedented applications: the substitution of individual metal nodes with secondary building units (SBUs), such as metal carboxylate clusters, represents a precise and potent technique to confer the resultant frameworks with enduring porosity and rigidity. This, in turn, elevates thermal stability and molecular complexity. [7,24,25] Catenanes made of MOCs

Recently, an advancement in this field has emerged through the integration of MOCs in polymeric structures by interlocking 0D MOCs into extended structures, yielding materials with properties combining those of MOCs and coordination polymers. In particular, their porosity is maintained, and their structural stability is enhanced by interlocking the 0D cages. Thus, host-guest chemistry can be studied and applied in this class of supramolecular materials.

Synthesis of Catenanes from MOCs

Despite it is still an emerging field of research, hence there are challenges to overcome in terms of designing suitable components, optimizing threading conditions, and characterizing the resulting structures, some notions can be disclosed.

While the direct synthesis of catenanes using MOCs as building blocks is a challenging task due to the inherent complexity of both structures [7], researchers have explored the incorporation of MOCs into catenane-like arrangements using templating strategies. *Templating with MOCs* represents a powerful strategy for synthesizing Catenanes [7]. Pre-formed MOCs, with their well-defined pores, guide the threading and interlocking of other molecular components; the pores within MOCs act as

scaffolds where additional molecular rings or components can thread through, resulting in the formation of interlocked architectures. The templating approach heavily relies on *host-guest interactions*. Guest molecules, are threaded through the pores of MOCs with the aid of various non-covalent interactions (such as hydrogen bonding and weaker electrostatic interactions).

Cornerstones about Catenated MOCs

In 1999, Fujita et al. made a groundbreaking contribution to the field of catenane synthesis by introducing the concept of creating interlocked molecules based on discrete 3D MOCs [25,26]. This work laid the foundation for subsequent explorations into MOC-based catenanes. Fujita's approach involved utilizing MOCs as building blocks for constructing mechanically interlocked structures, particularly [2]-catenanes. Fujita's pioneering work focused on the creation of discrete [2]-catenane structures using MOCs. These [2]-catenanes consist of two interlocked cages mechanically linked through the windows of the MOCs. By thoughtfully designing the MOCs and the threading components, Fujitademonstrated the feasibility of crafting these mechanically interlocked architectures. The achievement of creating catenanes from MOCs represented a significant departure from traditional catenane synthesis methods, which often involved complex and intricate chemical reactions. The introduction of templating strategies using MOCs as hosts further expanded the possibilities for creating interlocked structures precisely. [12,25–31]

In 2010, *Lu et al.* reported the synthesis of *the first infinite 3D cage-based polycatenane.* This architectural marvel was constructed by mechanically interlocking all polyhedral adamantane-like MOC vertices. Lu's groundbreaking work showcased the feasibility of producing intricate mechanically interlocked structures with the inherent porosity of MOCs. This advance catalyzed a surge of interest in the field, propelling researchers to explore new horizons in polycatenane synthesis. [10]

Dehnen and the Strand-Like Polycatenane. Dehnen and his team contributed to the expanding repertoire of polycatenane structures by introducing a strand-like polycatenane built from neutral icosahedral cages [2]. This marked the first example of a 1D MOC infinite catenation, ushering in the possibility of generating extended linear interlocked architectures. Dehnen's work underscored the versatility of MOCs as building blocks for diverse polycatenane structures, offering a glimpse into the potential applications of these materials. [32]

Lu's Tetrahedral MOC-Based Polycatenane. Lu et al. continued their exploration into polycatenanes with a pioneering report in 2012 [3]. They introduced both 1D and 3D polycatenane structures based on discrete tetrahedral MOCs. This work exemplified the importance of tailoring MOC geometries for achieving specific polycatenane

architectures. The resulting structures showcased dynamic pores and distinct adsorption properties, revealing the multifaceted nature of MOC-polycatenanes. [10]

Hong Group's Polycatenane Networks. The Hong group made significant strides in the realm of MOC-based polycatenane networks: through strategic design and careful selection of ligands, they generated two distinct cage-based infinite polycatenanes triggered by different anions. Their work shed light on the criteria necessary to induce the formation of intricate interlocked structures. By leveraging anion-temperature-induced approaches, the group demonstrated the ability to selectively produce kinetic polycatenanes over thermodynamically controlled products. [6]

Icosahedral Polycatenated Framework. In 2015, Zhao and colleagues pushed the boundaries of polycatenane synthesis by reporting a 3D polycatenated framework based on icosahedral MOCs [5]. Through propagated octuple intercatenation, they achieved the highest known catenation fold for 3D extended polycatenanes. Zhao's work showcased the intricate and versatile nature of MOC-based polycatenanes, revealing the potential for creating diverse and complex interlocked architectures. [8]

1.2. Coordination Polymers

While the concept of polymers was introduced by Berzelius in the 19th century, the term "coordination polymer" emerged in the early 20th century, describing cobalt(II) ammine nitrates. These materials gained attention and prominence in the scientific literature from the 1950s onward. It is noteworthy that the nomenclature 'coordination polymer' has endured and is embraced in contemporary polymer chemistry textbooks. Coordination Polymers (CPs) also referred as Coordination Networks (CNs) are intricate classes of materials that arise from the coordination of metal ions or clusters with organic ligands. In this thesis the term CPs is used to describe the extended structures that are different from the poly-[*n*]-catenanes made of interlocked cages.

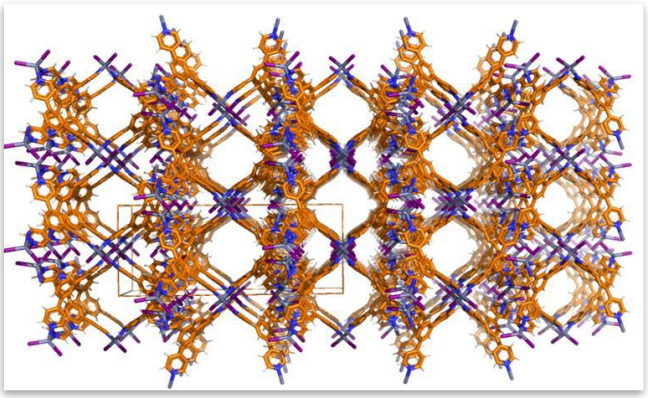

Figure 2 *Homemade example of CP: crystal packing of ZnI2-TPB-mX Coordination Polymer in single crystal form, with the voids forming the 1D channels expanding along the c-axis[30]*

Coordination Polymers and Coordination Networks

Coordination Polymers (CPs) are labelled as: "*A coordination compound with repeating coordination entities extending in 1, 2, or 3 dimensions*"[4]. They are a class of materials which are composed of metal ions or clusters linked by organic ligands through weak electrostatic interactions (such as Hydrogen bond). To be clear, a *coordination entity* is an ion or neutral molecule that is composed of a central atom, usually that of a metal, to which is attached a surrounding array of atoms or groups of 'N atoms, each of which is called a ligand.' **Coordination Networks** (CNs) are, instead, described as "*Coordination compounds extending, through repeating coordination entities, in 1 dimension, but with cross-links between two or more individual chains, loops, or spiro-links, or a coordination compound extending through repeating coordination entities in 2 or 3 dimensions*". It is clear that CNs and CPs are very similar, nearly concident, but the former is more extensive than the latter (i.e. the latter is a subclass of the former).

Key Features and Structural Diversity

The key aspects of CPs and CNs include their ability to exhibit an array of topologies, porosities, and functionalities based on the choice of metal ions and ligands. This diversity enables tailoring of properties for specific applications, such as gas storage, catalysis, and drug delivery. The porosity of CPs and CNs arises from the arrangement of metal-ligand coordination bonds, leading to potential guest molecule encapsulation within their cavities. To have a flavour of the structural diversity and versatility of CPs, we can consider, for instance the following structures: $[Cu(CN)]_n$, $\{Co(en)_{32}\}_n$, $\{[Mn(bpy)_2]Cl_2\}_n$, $\{[Cd(SCN)_2(py)]\}_n$ or $\{[Ag(NCS)]\}_n$.

$[Cu(CN)]_n$. This coordination polymer is characterized by its simplicity yet fundamental significance. It is formed by the coordination of copper ions (Cu^{2+}) with cyanide ligands (CN^-), resulting in the formation of a linear 1D chain structure. While not exhibiting the intricate porosity seen in MOFs, this example highlights the essence of coordination chemistry—how metal ions and ligands interact to generate ordered structures. This basic structure serves as a foundational illustration of how metal-ligand coordination can lead to the assembly of repeating units, forming a coordination polymer. [33,34]

$\{[Co(en)_3](NO_3)_2\}_n$. In this case cobalt ions (Co^{2+}) are coordinated with ethylenediamine (en) ligands and nitrate anions (NO_3^-). The resulting structure manifests as a 1D chain. The utilization of different ligands and counterions showcases the ability to tune the properties and structures of coordination polymers. The coordination of en ligands, which provide chelating sites, emphasizes the role of multidentate ligands in generating extended structures. [35,36]

$\{[Mn(bpy)_2]Cl_2\}_n$. A coordination polymer involving manganese ions (Mn^{2+}) coordinated with bipyridine (bpy) ligands and chloride ions (Cl^-), leading to the

formation of a 1D chain structure. The use of bpy ligands, known for their versatile coordination behavior, illustrates the impact of ligand choice on the structure. Additionally, the presence of counterions (Cl^-) highlights the influence of different anions on the coordination mode and topology of the polymer. [37]

{[Cd(SCN)$_2$(py)]}$_n$. This example showcases the coordination of cadmium ions (Cd^{2+}) with thiocyanate ligands (SCN^-) and pyridine (py) ligands. The resulting structure forms a 2D network. This case underscores how the combination of different ligands can lead to distinct coordination environments and dimensionality. The presence of SCN^- ligands, with their flexible coordination modes, contributes to the formation of extended structures. [38]

{[Ag(NCS)]}$_n$ is a coordination polymer which involves silver ions (Ag^+) coordinated with thiocyanate ligands (NCS^-), forming a 1D chain structure. Despite its simplicity, this example showcases the concept of metal-ligand coordination and how it can lead to the assembly of linear chains. The coordination of NCS^- ligands, with their anionic nature, illustrates the role of charge balance in coordination polymer formation.[39]

Essentially, in all of these cases the formation of CPs arises from the interaction between metal ions and ligands, resulting in ordered and extended structures. While these structures might not exhibit the same degree of porosity as MOFs, they exemplify the fundamental principles of coordination chemistry and how they can be harnessed to create materials with tailored properties. Each case underscores the importance of ligand choice, metal coordination geometry, and counterions in shaping the structure and properties of coordination polymers.

Analogies and Differences with MOFs, MOCs and poly-[*n*]-catenanes

While both CPs and MOFs exhibit the common characteristic of metal-ligand coordination, their distinctions lie in structural characteristics and porosity. MOFs generally possess higher porosity due to their large, well-defined cavities. In contrast, CPs and CNs often display greater structural diversity and connectivity, leading to intricate and varied frameworks. The distinction between these materials is not always rigid, as some CPs can exhibit MOF-like porosities, blurring the boundaries between the two classes. Poly-[*n*]-catenanes areMIMs formed by the interlocking of multiple molecular strands. Unlike CPs and CNs, which form extended solid structures, poly-[n]-catenanes are more akin to discrete molecules. Metal-organic cages (MOCs), on the other hand, represent confined structures where metal ions and ligands assemble to encapsulate guest molecules. The distinction lies in the encapsulation pattern: CPs and CNs emphasize extended networks, whereas MOCs show discrete, encapsulating geometries [40]

1.3. Nature and behaviour of $M_{12}L_8$ poly-[*n*]-catenanes

1.3.1. The nature of $M_{12}L_8$ poly-[*n*]-catenanes

For the synthesis of the poly-[*n*]-catenanes studied in this thesis, tridentate ligands 1,3,5-tris(pyridin-4-yl)benzene (*i.e.* TPB) and 2,4,6-tris(4-pyridyl)pyridine (*i.e.*, TPP) have been self-assembled with ZnX_2 (where X = Cl, Br, and I). The synthetic approach used to self-assemble the organic ligands and metal ions has been using solution chemistry and solid-state reactivity. In particular, the solution approach consists of using slow crystallization (*i.e., three layer method*) and fast crystallization (*i.e., instant synthesis*) methods, while in the solid-state *neat grinding* has been exploited following the mechanochemical approach [4,5,41]. In this way, building blocks (in this case, if polycatenanes are formed, the building block are $M_{12}L_8$ nanocage, as seen in ***Figure 3***) organize following a **self-assembly process** involving coordination bonds, hydrogen bonding and π-π interactions of the aromatic rings with the guest molecules which drive the structure formation [42]. For more information, refer to the HSAB theory, which determines the formation of stronger or weaker links between organic and inorganic counterparts and thus the stability of the material. [42,43]

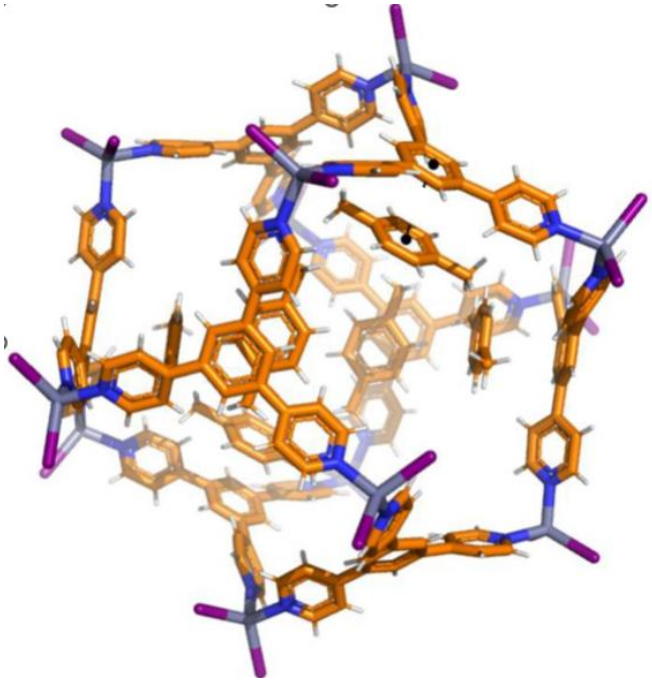

Figure 3 *icosahedral nanocage $M_{12}L_8$ (i.e., a poly-[n]-catenane unit)*

Thermodynamic versus kinetic reaction control

Thermodynamics and kinetics are two fundamental and complementary concepts that elucidate different aspects of chemical reactions, governing the reaction outcome and the distribution of resulting products. Regardless the general theory and referring, in

particular, to *thermodynamic versus kinetic control*, this concept represents one of the milestones of our activity.

Thermodynamic control relates to situations where the stability or free energy of the products dictates the reaction. It implies a preference for the formation of the most thermodynamically stable product. Typically, this occurs under equilibrium conditions, where an **error-checking process** allows to break up chemical bonds of an assembled structure which is not, however, stable enough, and this happens until the most stable structure is eventually achieved. This enables the system to reach its lowest energy state [20,44]. In our case, the thermodynamically controlled product is favored for long reaction times. We will see that, amongst the three methods to synthetize a catenane, just one gives *the thermodynamic product*.

Conversely, kinetic control focuses on the influence of reaction rates on the product distribution. Here, the reaction is governed by the kinetics (i.e. the reaction rate), rather than the stability of the products. Kinetic control is commonly observed when the reaction does not achieve equilibrium (e.g. short times or irreversible processes): in that case, the kinetic product is favored as it forms more rapidly, even though it may not be the most stable.

We will see that, amongst the three methods to synthetize a catenane, two of them give *the kinetic product*.

1.3.2. The behaviour of $M_{12}L_8$ poly-[*n*]-catenanes

Host-guest chemistry

The most notable peculiarity of MOF and, similarly, a fundamental characteristic of poly-[n]-catenanes is the so-called **host-guest chemistry**. That is essentially the topic of all our activity.

Because of the existence of nanocages with each structure and throughout the chains, the host-guest chemistry in catenanes involves the interaction between the interlocking rings or components of the structure and guest molecules that can bind or be encapsulated within the cages [4,13,14].

In this context, the polycatenane acts as the host molecule, providing a cavity or **binding site** where guest molecules can be accommodated. The interlocked structure of the catenane introduces specific spatial constraints and geometric preferences that influence the binding of guest molecules, leading to the so-called **molecular recognition**: selective binding and recognition of guest molecules based on their size, shape, or chemical properties can occur. In particular, due to the presence of benzene

and pyridine rings, the internal $M_{12}L_8$ surface is embedded with aromatic binding sites that influence molecular recognition [3]. Moreover, Solid-state NMR reveals a quite weak signal belonging to the quaternary atoms of the benzene ring (136-129 ppm) compared to that of the quaternary atoms of pyridines (150-147 ppm), clearly showing the static behaviour of the benzene ring; this, therefore, serves as a good anchoring point for defining the molecular rotor axis. [3,45]

The chemical interactions involved are hydrogen bonding, van der Waals forces, and especially π-π stacking interactions (e.g. aromatic rings, as it will be widely discussed later on). These interactions contribute to the stability and specificity of the host-guest complex, enabling eventual selectivity of the cages towards different molecules (e.g. xylene isomers). But what is exactly the mechanism thanks to which guests can be uptaken in the cages? Does the catenation structure remain intact after the release of templating guests?

The experimental results show that despite the absence of continuous channels, the $M_{12}L_8$ catenanes can still uptake guest molecules [5]. This is achieved through dynamic behaviour and concerted displacements of the catenated cages, allowing temporary access to the internal voids where guests can be included.

Crystallinity aspects: from *templating effect* to *SCSC and CAC processes*

As seen, the solid-state synthesis of pol-[*n*]-catenanes is able to produce mechanically interlocked, porous supramolecular structures. These structures are stable either thermodynamically or kinetically, and they can result in amorphous or crystalline matter, powder or crystal form. Nevertheless, mechanical forces produce mechanical bonds that intricately link the constituent parts of the Catenanes, but it is polar guests (which exhibit intermolecular interactions) that effectively stabilize and template the mechanochemical synthesis of crystalline formations. [5,46,47]

Aromatic solvents (like nitrobenzene or dichlorobenzene) have high molecular dimensions and exhibit π-π interactions. These interactions stabilize and template mechanochemical synthesis crystalline formations, on one hand (aromatic solvents in the reaction mixture promote interconnected $M_{12}L_8$ nanocages and organized crystalline domains *during self-assembly*) and aromatic solvents (or *guests*) provide strong van der Waals interactions between ligands in nanocages, in the other hand (resulting in well-defined crystalline catenated cages *after the formation*).
Conversely, non-aromatic solvents have smaller molecular dimensions and weaker aromatic interactions (e.g. chloroform or methanol), hence lower stabilizing and **templating effects** – or, even, the lack of π-π interactions in non-aromatic solvents might hinder nanocage interlocking formation and hamper the creation of ordered crystalline structures [48]. Thus, as will be widely discussed in *Results and Discussion*, mechanochemical synthesis in non-aromatic solvents generates amorphous products.

In this context, the **single-crystal-to-single-crystal** (**SCSC) process** is a term used to describe a phenomenon wherein a crystalline material transforms from one crystal lattice structure to another, while maintaining its single crystal form throughout the transformation [29]. This means that the material changes its arrangement of atoms or molecules without undergoing any disruption to its overall crystalline integrity. Importantly, this happens through exchange of the guest molecule inside the host material's crystal lattice (i.e. **Guest Inclusion** or **Guest Exchange**), without affecting its structure. The process is reversible, and weak intermolecular interactions (e.g. hydrogen bonding, van der Waals forces, or π-π stacking) enable this exchange. Considering the nature of interlocked catenated MOCs of our material, this is a paramount property. [20,29]

Exactly similarly, the **crystalline-to-amorphous-to-crystalline (CAC) process** consist of the transformation of a crystalline material into an amorphous phase and its recrystallization. This process can lead to the formation of *new* thermodynamically stable phases. Essentially, given a specific crystalline MOF or MOC, upon exposure to specific conditions (such as elevated temperature), the material undergoes a phase transition into an amorphous state. In this state, the material lacks the long-range order of a crystal lattice. As the material continues to be exposed to high temperature, the amorphous phase begins to reorganiz. Eventually, the material recrystallizes into a new crystalline phase, which have a different structure and properties compared to the initial one. Firstly and foremost, CAC process is notable since it provides insights into the relationships between structure and properties in materials. [20,46,48]

2 MATERIALS AND METHODS

Starting materials and solvents were purchased from commercial suppliers (Alfa Aesar, Apollo Scientific, Fluka, FluoroChem, Honeywell, Sigma Aldrich, TCI, iChemicals) and used without further purification, if not mentioned otherwise.

2.1. Materials: Analytical Instrumentation

Powder X-Ray Diffraction

Bruker D2-Phaser diffractometer equipped with Cu radiation (λ = 1.54184 Å) using Bragg Brentano geometry. The experiments were performed at room temperature.

Single Crystal X-Ray Diffraction

Single crystal X-ray data of poly-[*n*]-catenanes were recorded using a XtaLAB Synergy-S, Dualflex, HyPix-6000HE diffractometer. Suitable crystals are mounted on a suitable support, cooled down at 173 K for data collection and the structure is solved with the *ShelXT structure solution* program using the *Intrinsic Phasing solution* method and by using *Olex2* as the graphical interface. The model is refined with *version 2014/7 of ShelXL* using Least Squares minimization. [2]

Nuclear Magnetic Resonance (NMR)

Bruker ARS (400 MHz) spectrometer, once selected an appropriate number of scans and relaxation time using several deuterium solvents depending on the compound to be analyzed (above all, D_2O, $CDCl_3$,DMSO).

2.2. Methods: synthesis of catenanes and ligands

Four ways of synthesis of $M_{12}L_8$ poly-[*n*]-catenanes have been carried out, roughly classified as *fast methods* or *slow methods*, according to the rate of growth of the crystals

they can guarantee (i.e. the kind of product, thermodynamic or kinetic, it is expected); whilst ligand synthesis has been performed via a *Suzuki-Miyaura Coupling*.

Catenane synthesis via *Three-layer method*

Stoichiometrically, since the general formula of catenanes is $M_{12}L_8$ thus the ratio ligand to metal is 1:1.5. Taking as basis 30 mg of ligand, the quantities must be therefore:

- 30 mg TPB (MW = 309.364 g/mol) = 0.097 mmol * 1.5 = 0.1455 mmol
- 46.444 mg ZnI_2 (MW = 319.2 g/mol)
- 32.767 mg $ZnBr_2$ (MW = 225.2 g/mol)
- 19.829 mg $ZnCl_2$ (MW = 136.3 g/mol)

In a 25 mL round-bottomed flask 30 mg of TPB is suspended in X mL of solvent. Then, 2 mL of CH_3OH is added and the mixture is stirred at room temperature until a clear homogeneous solution is obtained. Meanwhile, a given amount of metal salt ($ZnBr_2$ = 32.76 mg, $ZnCl_2$ = 19.83 mg, ZnI_2 = 46.43 mg) is dissolved in 1 mL of CH_3OH in a glass vial. The ligand solution is transferred to a test tube and 3 mL of methanol is very carefully dripped to allow the stratification of the solvents. Then, the metal solution is carefully added to create the third layer, and the test tube is closed to avoid solvent evaporation. Single crystals formed in about 1 week as yellowish transparent crystals.

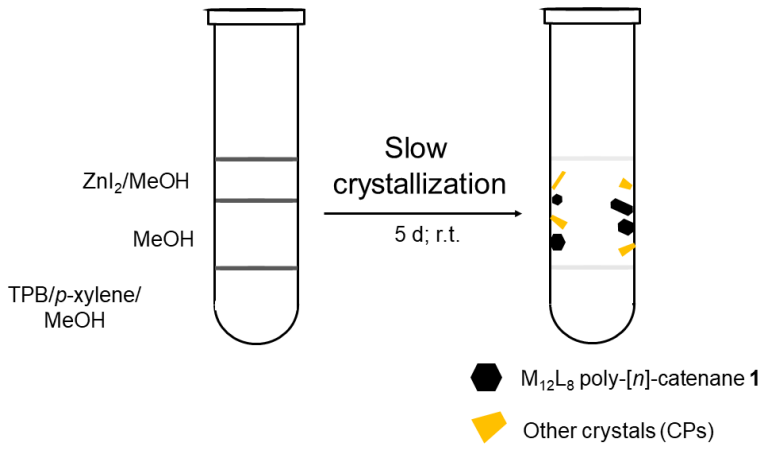

Figure 5 *Cartoon representing the slow crystallization method* [2]

Catenane synthesis via *Instant synthesis*

This *fast method* allows the selective synthesis using kinetic control. Stoichiometric quantities are the same declared above. Crystalline powder is obtained upon the addition of metal salts.

In a 25 mL round-bottomed flask, 30 mg of TPB are suspended in X mL of solvent. Then, 2 mL of CH_3OH is added and the mixture is stirred at room temperature until a clear homogeneous solution is obtained. Meanwhile, a given amount of metal salt ($ZnBr_2$ = 32.76 mg, $ZnCl_2$ = 19.83 mg, ZnI_2 = 46.43 mg) is dissolved in 1 mL of CH_3OH in a glass vial. The metal solution is quickly poured into the ligand solution under vigorous stirring. After the addition of the metal salt, a white precipitate immediately forms giving a suspension which is left stirring for 15 minutes. The formed solid is finally filtered and left to get dry.

Catenane synthesis via *Neat grinding*

This is a second *fast method* (so, kinetic control is achieved) which differ from the previous one in the absence of solvent. The product is an amorphous powder as no solvents are added as templating agent.

In the solid-state reaction, 30 mg of TPB and a given amount of metal salt ($ZnBr_2$ = 32.76 mg, $ZnCl_2$ = 19.83 mg, ZnI_2 = 46.43 mg) are grinded in a mortar for 30, 60 minutes to obtain a powder solid. The reaction was monitored by powder XRD (hereafter, P-XRD) by checking how the diffraction peaks of the TPB ligand disappeared completely.

Catenane synthesis via *Solid-liquid interphase*

An alternative method to instant synthesis is the solid-liquid interphase method. It differs in that no ligand solubilization is needed and the methanolic solution of metal salt is instantaneously added. This is particularly useful, for instance, when the ligand is insoluble in the desired guest.

In a 25 mL round-bottomed flask, a mixture of solvent and CH_3OH. is added and stirred at room temperature. Then, 30 mg of TPB and a methanolic solution of metal salt (1 mL of CH_3OH in $ZnBr_2$ = 32.76 mg, $ZnCl_2$ = 19.83 mg, ZnI_2 = 46.43 mg) are simultaneously poured into the flask under vigorous stirring. A white precipitate immediately forms giving a suspension which is left stirring for 1-2 hours. The formed solid is finally filtered and left to get dry.

Guest inclusion (or *exchange*) process

To study the guest behavior of the synthesized materials, 30 mg of the poly-[*n*]-catenane in powder form are added in a round-bottom flask with 5 mL of the guest material. The system is stirred for a given amount of time, typically overnight. Then, the stirring is stopped to let the solution settle. The mixture is filtered, and the resulting solid is left to get dry (to speed up the process, it is possible to use N_2 flux).

Adsorption column

A glass-made Pasteur pipette is fixed vertically and a small piece of cotton is pushed on the bottom of to avoid any solid leakage (Figure 2). As basis of calculus, 100 mg of catenane in powder form is carefully packed into the pipette. Then, 2 mL of chloroform and 2 mL of methanol are poured in the pipette both to 'wash the powder' from unreacted reactants and to pack more finely the *adsorption bed*. The system is left to percolate down the pipette through the solid and collected in a vial below. Procedure is repeated with 2 mL of chloroformic NB mixture. Once all the liquid is passed through, the solid is left to get dry and both parts analyzed (through P-XRD and/or NMR).

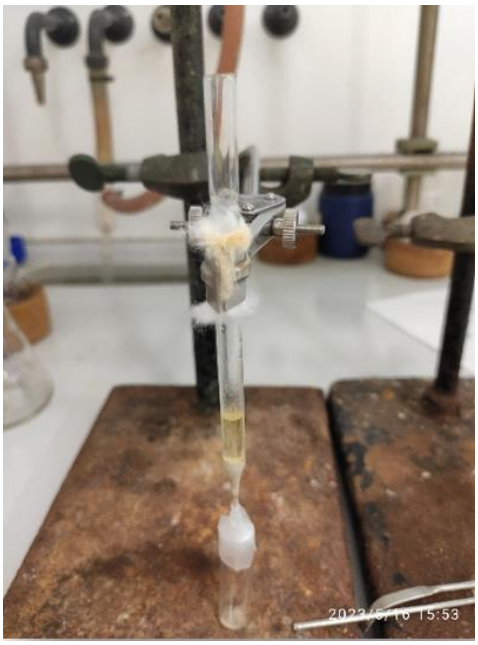

Figure 4 *Picture of a rough 'adsorption column': a glass-made Pasteur pipette filled with catenane in powder form*

Ligand synthesis through *Suzuki-Miyaura Coupling*

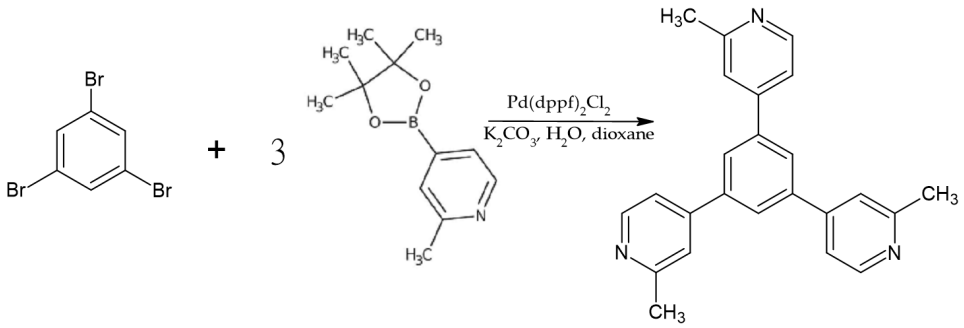

3-Br Benzene 2-met-Pyr-Boronic esther mTPB

To synthetize 4,4'-(5-bromo-1,3-phenylene)dipyridine, in a 500 mL two-necked round-bottom flask dioxane (153.6 mL) and a solution of K_2CO_3 (11.24 g, 81.4 mmol) in H_2O (40.7 mL) are added and degassed for 10 minutes. Then 1,3,5-tribromobenzene (2.56 g, 8.14 mmol), 4-pyridineboronic acid pinacol ester (1) (5 g, 24.41 mmol, 3Eq), tricyclohexylphosphine (684 mg, 2.44 mmol) and [1,1'-bis(diphenyl-phospino)ferrocene]palladium(II) chloride (893 mg, 1.22 mmol, 15 mol%) are added. The mixture is degassed under stirring for further 10 minutes and then refluxed under nitrogen atmosphere for 48 h. The completion of the reaction is checked by TLC, then the mixture is cooled to room temperature and 100 mL of dichloromethane is added. The organic phase is separated and washed with H_2O (2x40 mL), dried over Na_2SO_4, and the solvent is removed under reduced pressure to yield a dark brown oil. The crude is purified by flash column chromatography on silica (DCM:TEA=97:3) to yield 1,3,5-tri(pyridin-4-yl)benzene as a white solid. [49]

3 RESULTS AND DISCUSSIONS

The aim of this thesis is to expand the research carried out in poly-[*n*]-catenanes self-assembled on interlocked $M_{12}L_8$ nanocages, both understanding their guest behaviour and exploring new ligands as building blocks. Firstly, synthesis and characterization of a new ligand, in a perspective of diversification of catenanes precursors. Secondly, assessment of the behaviour of that new ligand while involved in poly-[n]-catenanes formation; what will be the resulting behaviour? Thirdly, looking into the selectivity of these Metal-Organic Cages towards some key-compounds: from xylenes isomers to nitro-contaminants, to name a few, exploiting in this way the property of molecular recognition within their host-guest chemistry.

3.1. Selectivity of Catenanes in crystal form

Justification

As widely discussed in the *Introduction*, on the one hand polycatenanes are hollow molecules[1] with the ability to encapsulate up to 12 guest molecules within the $M_{12}L_8$ cavities (such as in the case of $(ZnBr_2)_{12}(TPB)_8$), and on the other hand isomer separation or contaminant sequestration are topics of significant industrial interest. Thus, it is worth exploring the possibility of creating materials that act as filters with selectivity towards specific chemicals *exploiting the isomer recognition property*. This field of research is about molecular recognition.

Proof of Guest Exchange

The amorphous $(ZnI_2)_{12}(TPB)_8$ poly-[n]-catenane in powder form is readily synthesized in the solid-state through *neat grinding* (see *Materials and Methods*), and the resulting powder X-ray diffractogram is shown in ***Figure 5***.

[1] Unit cell volume: 20000 Å^3 [2]. Internal volume per nanocage: 2600-2700 Å^3 [2–4].
Degree of void per unit volume: 21-38 % [2].

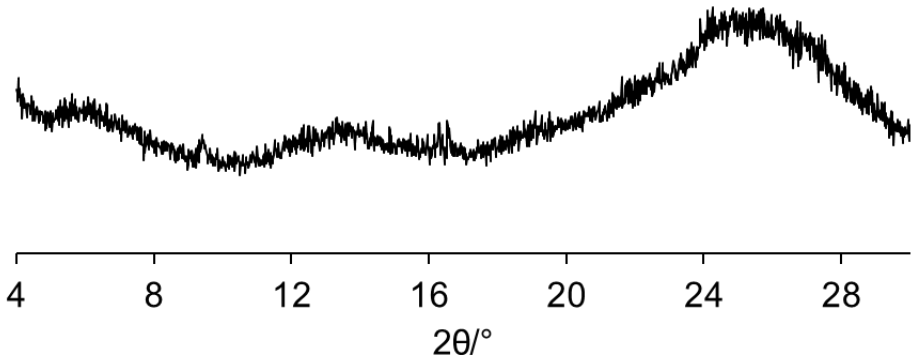

Figure 5 *Amorphous* $(ZnI_2)_{12}(TPB)_8$*, powder form*

Thanks to which it is possible to stand out the amorphous state because of the total absence of sharp peaks. Interestingly, thehilly profile reveals a short-range order. Indeed, the lack of guest inside the cages – which would act as **templating agent** – allows the supramolecular structure to emerge, but it immediately collapses.

The guest inclusion experiment was carried out by immersing the amorphous phase in 8 mL of paraxylene (hereafter, *p*X), together with 2 mL of methanol as templating agent. After filtration the solid showed the corresponding pattern as shown in ***Figure 6***.

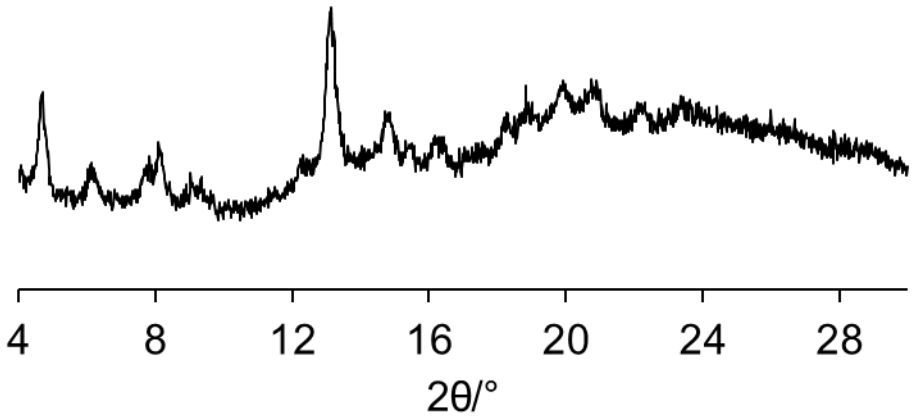

Figure 6 *P-XRD after GI with pX*

The emergence of peaks is self-evident and the powder can be considered (at least partially) crystalline. As footnote, consider that a longer exposition or a better templating guest would have led to a more crystalline pattern.

Finally, an overnight soaking of 100 mg of this powder (which includes *p*X) in 8 mL of 1,2-dichlorobenzene (hereafter *o*-DCB), together with 2 mL of methanol, proves the guest exchange since the P-XRD pattern is clearly different (***Figure 7***).

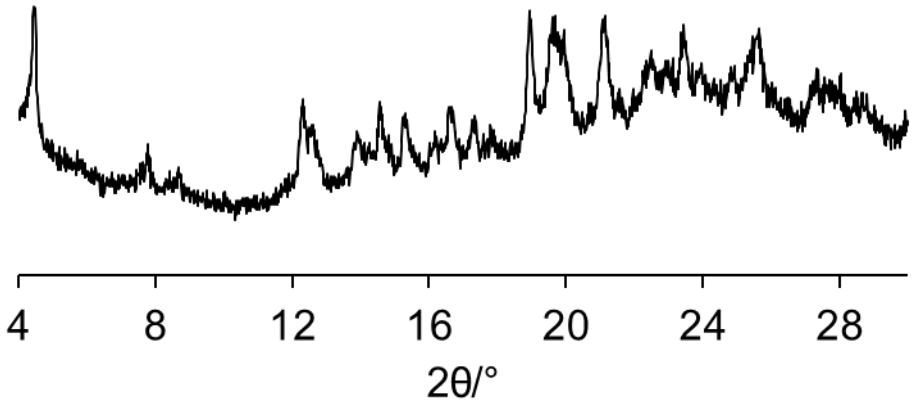

Figure 7 *P-XRD after GE between pX and o-DCB*

Crystal characterization of xylenic $M_{12}L_8$

The study of catenanes selectivity in crystal form require, first of all, the preliminary knowledge of their crystallographic features. We need, in other words, to access to the microscopic structures of catenanes. Hence, a TPB-ZnI_2 $M_{12}L_8$ poly-[*n*]-catenane crystal suitable for SC-XRD analysis is needed. Slow crystallization by *Three-layer method* with $CHCl_3$ as guest, together with CH_3OH as *templating agent* was attempted – chloroform is non-aromatic and do not establish efficient electrostatic interactions, thus it is disordered in the $M_{12}L_8$ cages and so it is not detected in the SC-XRD data, however the $M_{12}L_8$ cages are formed and refined easily.

Thus, oX, mX, *p*X as templating solvents were used to let crystals grow for some weeks. While the poly-[*n*]-catenanes in *p*X crystallized in just 5 days, giving single crystal suitable for SC-XRD., so far for the samples with *o*X and *m*X only CPs were obtained.[2] This observation must be attributed to the poor ability of *o*X and *m*X as templating agents, differently from *p*X. This, in turn, is closely linked to the geometry of these aromatic hydrocarbons (steric hindrance lets guests enter and be stabilized more or less easily).

Eventually, once properly grown up all the three structures has been analyzed by SC-XRD. Here, the most remarkable aspect is that this is the first documented case where the whole available space inside $M_{12}L_8$ nanocages is occupied by ordered *p*X guest (i.e. the maximum *guest uptake* has been achieved for an aromatic molecule).
For the sake of example, the $[(ZnI_2)_{12}(TPB)_8]_{12}$(*p*X) crystal characterization will be presented.

The 173 K SC-XRD analysis of the abovementioned structure crystallizes in the **trigonal system** in the rhombohedral **R-3 space group** with the following lattice parameters:

$$a = 38.8631(6)\ \text{Å},\ b = 38.8631(6)\ \text{Å};\ c = 16.2355(3)\ \text{Å}\ ;\ \alpha = \beta = 90°,\ \gamma = 120°$$

and total volume V = 21235.9(8) $Å^3$, while the volume of each cage is 2719 $Å^3$ – which unambiguously let them be called *large cages*. The dimensions of the cage "from-roof-to-floor" along the *c*-axis are 20.216 Å before interlocking and 12.322 Å after the mechanical bond formation.

In the picture below (***Figure 8***) the resulting structure is shown viewed along the crystallographic *c*-axis, A single nanocage is shown in ***Figure 9***.

[2] The difference lies in the *kinetic vs thermodynamic product*. For more information, see the dedicated chapter in *Introduction*.

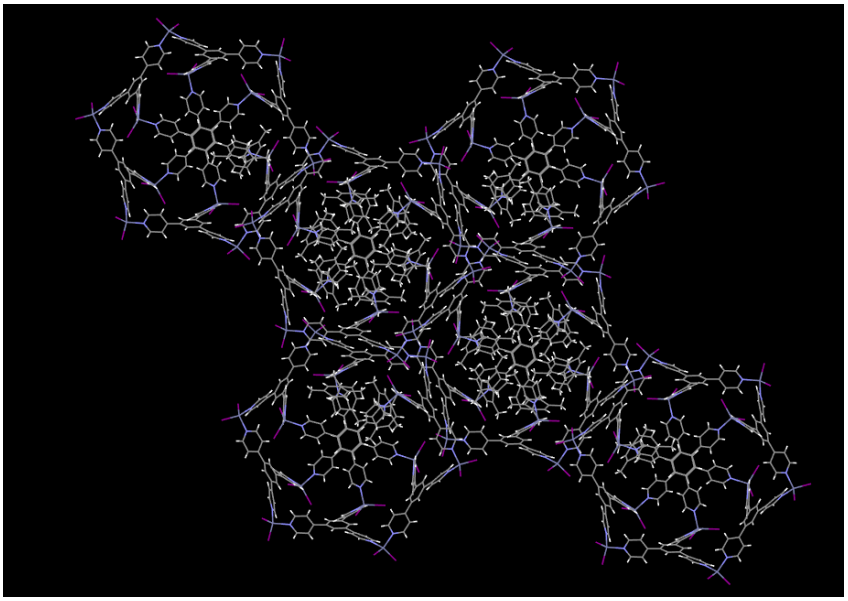

Figure 8 *Unit cell of ZnI_2-TPB-pX single crystal. Here it is possible to appreciate the 1D chain-like catenane*

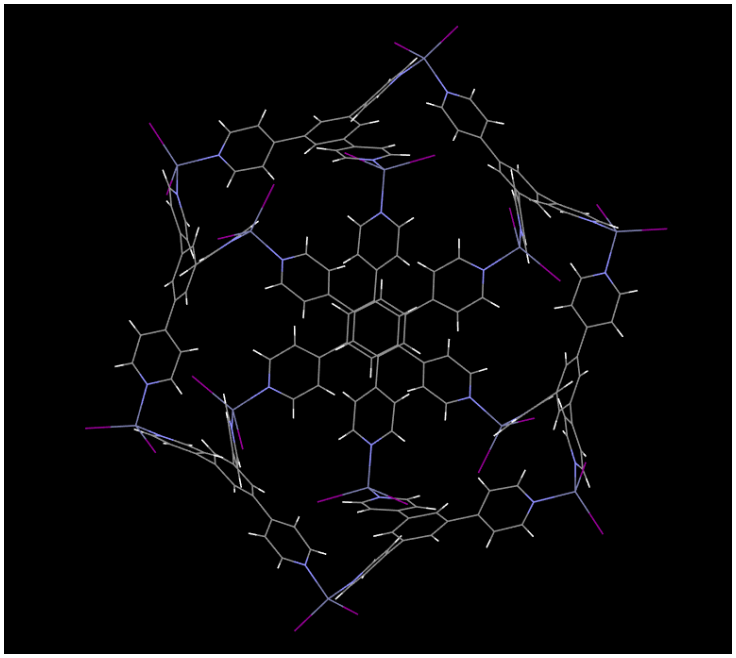

Figure 9 *ZnI_2-TPB-pX single crystal, single nanocage view*

There are two ZnI_2, one TPB, one third of a second TPB, together with two independent (from a crystallographic point of view) *p*X guests (hereafter labelled A and B) in the asymmetric unit as shown in Figure 8. The amount of space occupied by the guests is 38.4 % of the total unit cell volume (8176 of 2719 $Å^3$ per cage).

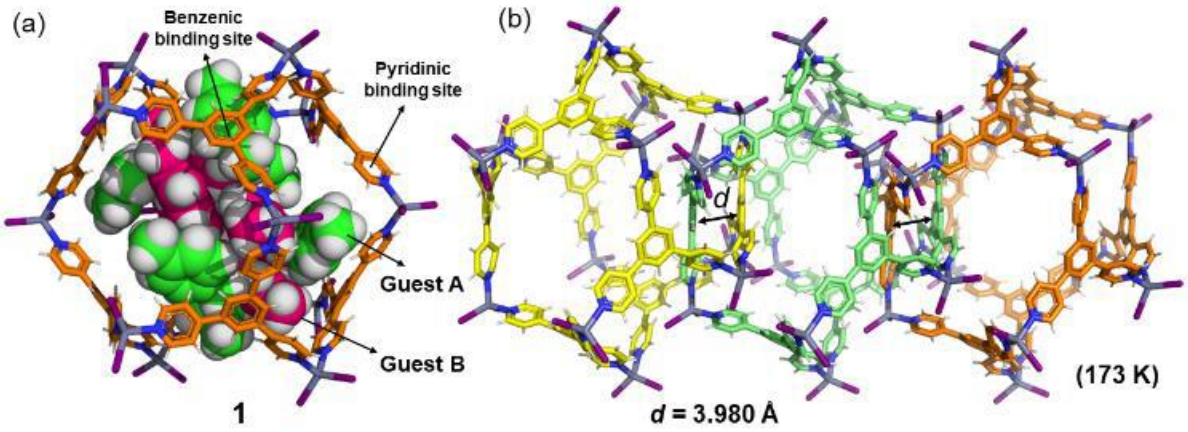

Figure 10 *Single, icosahedral nanocage (a) and 1D view along the plane a,b (cell vectors) (b) of* $[(ZnBr_2)_{12}(TPB)_8]_{12}(pX)$ *poly-[n]-catenane [3]*

Guests *p*X-A and *p*X-B are crystallographically different since the former lies near the walls and van der Waals forces are established with TPB (through aromatic-aromatic interactions), while the latter occupies the inner part of each nanocage. *p*X-A orientation is not perfectly parallel to the TPB rings.
Further crystallographic parameters such as distance among the closest benzene rings or pyridine-benzene torsion angles will be shown later – to better compare the SCSC processes.

Gas-Solid Guest Exchange

SCSC processes are fundamental to understand the guest uptake, reactivity and molecular recognition of crystalline, porous solids. [3,31,45,50]

The same single crystal $[M_{12}L_8](pX)_{12}$ previously examined by SC-XRD has been exposed to vapours of *o*-DCB for 6 days in a closed, room-T chamber (***Figure 11***). A shorter *o*-DCB exposition would lead to a smaller amount of guest uptake, and hence to a worse guest resolution via SCSC process.

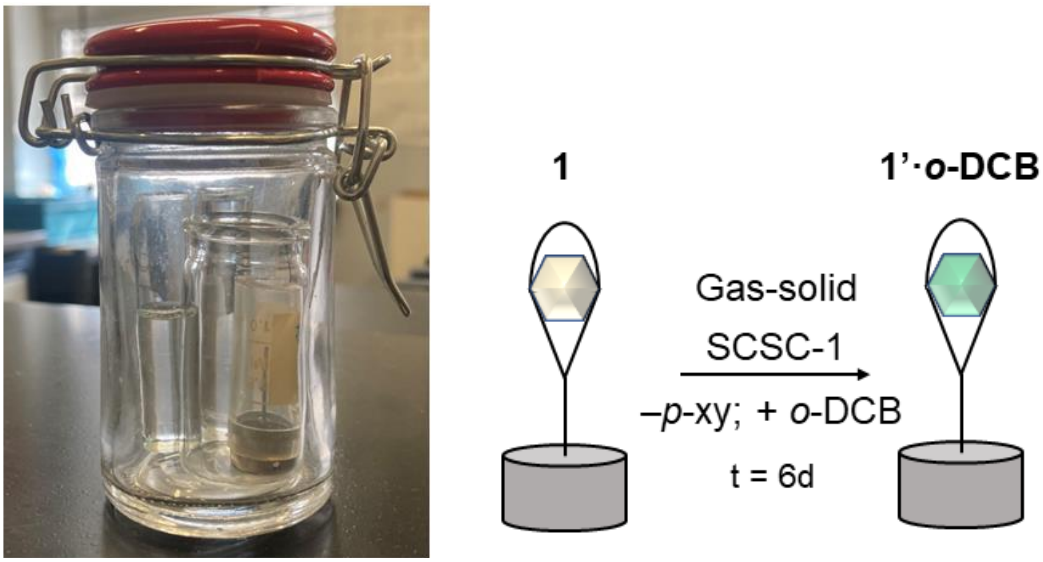

Figure 11 *Chamber containing the vials with the solvents used for SCSC process and Cartoon showing the SCSC [7]*

Notice that, beyond the advantage of having access to the crystal structure (differently from powder-form experiments) and of excluding recrystallizations, additional advantage of SCSC process is the gentleness of the GE – a liquid-solid one is much faster and aggressive, leading to the risk of damaging the crystals.

After the guest exchange, SC-XRD reveals a volume of 19884.7(7) $Å^3$ and the following lattice parameters:

$$a = b = 38.3737(6)\ Å\ ,\ c = 15.5927(3)\ Å\ ;\ \alpha = \beta = 90°\ ;\ \gamma = 120°$$

Thus, the process essentially consists in a slight c-axis shrinkage (0.6 of 16.2 Å, ca. 4% shortening of the channels), whilst the π–π host-guest distances remain almost constant (ca. 0.2% approaching). What significantly change is, instead, the microscopic configuration of rings inside the cages: angles between pyridine and benzene rings in each crystal are the following

	Bz1-Py1	**Bz1-Py2**	**Bz1-Py3**	**Bz2-Py4**
$[M_{12}L_8]\cdot_{12}(pX)$	36.93°	31.65°	20.06°	43.41°
$[M_{12}L_8]\cdot_6(o\text{-DCB})$	27.63°	43.9°	33.54°	37.18°

Table 1 *Angles between aromatic rings before and after SCSC process*

Eventually, from a guest uptake point of view the cages pass from 12, ordered *p*X molecules to just 6 *o*-DCB per nanocage[3] and *o*-DCB is under benzenic binding site of TPB, differently from *p*X which lies below the pyridinic one.

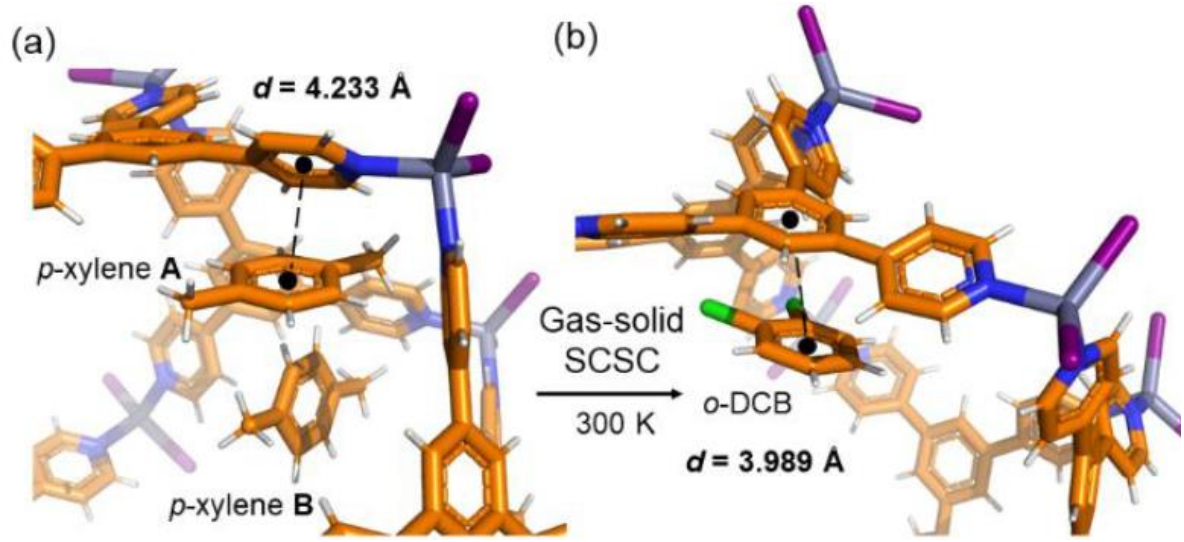

Figure 12 *Binding sites inside nanocages, before and after SCSC process*[3]

Multiple SCSC Guest Exchange. Selectivity. Host-guest chemistry

Once encompassed the *binding site* changes, the next aim os to test the *molecular recognition* abilities of the material. Exactly as before, the *Single crystal* of $[M_{12}L_8](pX)_{12}$ has been exposed to vapours of NB for 2 days in a closed, room-T chamber. SC-XRD confirms the SCSC process occurred successfully and the crystal underwent no damages.

The main difference from previous GE consist either in the speed (*one third of time*) and the degree of void (*21% vs previous 15%*), whereas both the number of guests (6) and the binding sites exploited (*below the benzenic ring of TPB*) are the same. Lattice parameters, nanocages framework and unit cell volume slightly shrink after the process, but less than the previous SCSC.

After that, subsequent SCSC processes are set up. $[M_{12}L_8](pX)_{12}$ has been exposed to NB for 18 h, than to equivolumetric mixture of *o*X, *p*X for 6 days. In this case, the

[3] Remember not the entire crystallographic structure can be disclosed: the main limitation often remains the identification of the inner content of each nanocage, due to its disordered nature.
Actually, it is possible to indirectly compute the disordered guest inside through *SQUEEZE procedure in the PLATON program of SC-XRD*, by the electron count within the M12L8 cages. This give a result of 2.5 *o*-DCB guests per nanocage.

binding sites change from pyridine to benzene to pyridine again (*i.e. the process is perfectly coherent*[4] *and reversible*).

There is, nevertheless, a remarkable difference. While this new *p*X coincides with the original *p*X -A, the inner *p*X -B is not observed. Thus, selectivity towards isomer seems prefer *p*X over *o*X (despite it is difficult to undoubtfully conclude so since, again, what happens in the inner, disordered part of cages is not accessible). Additionally, differently from *p*X, slow crystallization of single crystals grown with *o*X and *m*X tend to form 1D coordination polymers, which suggests that *p*X templates better the cages formation and - since they have both practically the same $\Delta E_{host\text{-}guest}$ – steric hindrance might be the key factor of selectivity.

Afterwards, this *p*X crystal was in turn exposed to equivolumetric mixture of *o*-DCB, NB: just NB entered.

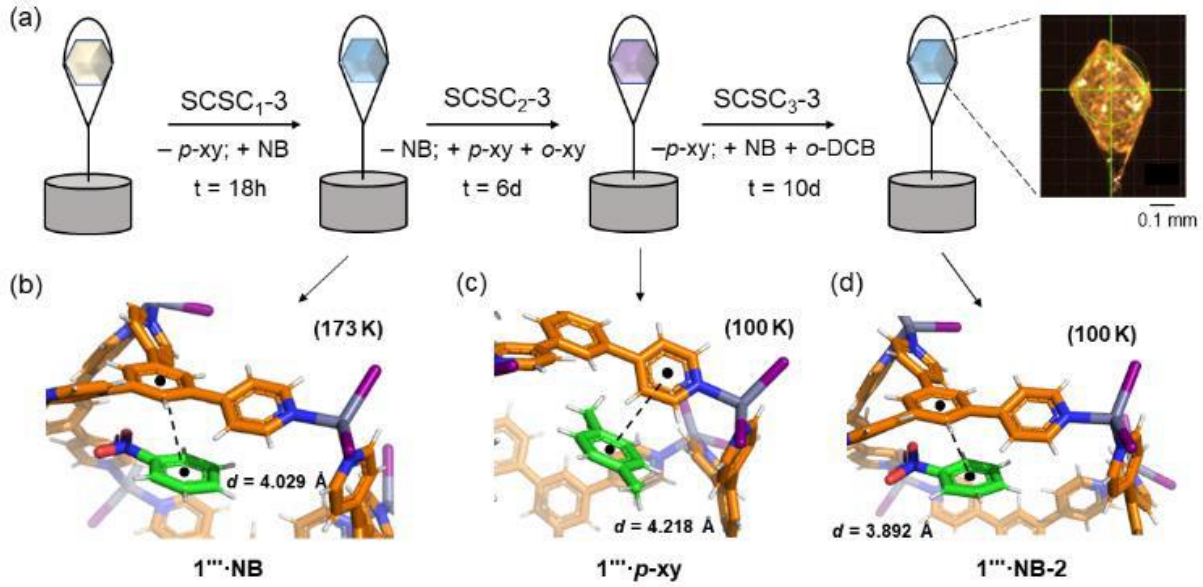

Figure 13 *Multiple SCSC experiments for different guest molecules, together with the virtual images of detailed host-guest interactions [3]*

For what concern *p*X and *o*-DCB, none of the previous crystals have been used: slow crystallization *with $CHCl_3$ as guest, methanol as adjuvant and paracetamol as templating agent* was attempted. Empty crystals (*i.e. disordered guest inside*) are revealed by SC-XRD. After subsequent exposition to *p*X/*o*-DCB vapours for 24 h, *p*X is entrapped.

[4] The position of pX entered in a **pre-formed Single Crystal** (i.e. *SCSC process*) is the same as obtained by **bottom-up self-assembly** (i.e. *Slow crystallization through Three-layer method*). Also host-guest π–π interactions are exactly the same.

Moreover, the quickness of the process shows the good affinity of our material towards *p*X. That is a remarkable result.

Last but not least, the litmus test of these results consists in computational calculations through *Density Functional Theory* (DFT) of host-guest interactions energy. It undoubtfully highlights that NB is the strongest embedded (44 kcal/mol), whereas xylenes isomers lie in about 35 kcal/mol and *o*-DCB is the weakest bonded (25 kcal/mol). These results must be coupled with geometric considerations (i.e. steric hindrance) to come up with the experimental results formerly showed (that is particularly true to explain the xylenes selectivity).Detailed crystallographic data can be found in *Appendix A*.

In conclusion, through slow crystallization methods it is possible to grow single crystals of $M_{12}L_8$ poly-[*n*]-catenanes. These MOCs have several binding sites in internal faces of icosahedral nanocages. These binding sites exhibit molecular recognition properties. In particular, the rotational behaviour of the TPB pyridine rings and the mechanically interlocked nature of these materials justify structural properties such as stability and robustness of the metal-organic framework, molecular recognition ability and structural responsiveness (i.e. dynamic behaviour [4]) upon guest absorption. Via SCSC guest exchange process, coupled with SC-XRD crystallography, it has been possible to proof the preferential uptake from gas phase of aromatic molecules such as pollutant NB or *o*-DCB, or discern amongst industrially relevant isomers. Thus, they have shown to be good candidates for molecular sieve applications, isomer separation or sensing applications of target aromatic molecules.

3.2. Selectivity of Catenanes in powder form

Whilst the study of $M_{12}L_8$ poly-[*n*]-catenanes is significantly more feasible in crystal form, its usage is much more viable in powder form, instead (at least in an engineering scale-up perspective. See *Applications: an engineering perspective*). Once demonstrated the selectivity of the former, it is reasonable to look into the latter.

Selectivity of amorphous powder towards isomers

Amorphous powder of ZnI_2-TPB catenanes can be readily synthesized through *neat grinding* or *instant synthesis* in chloroform and methanol. In this case, the second path was followed, and the crystallographic nature was easily confirmed by P-XRD (***Figure 14***).

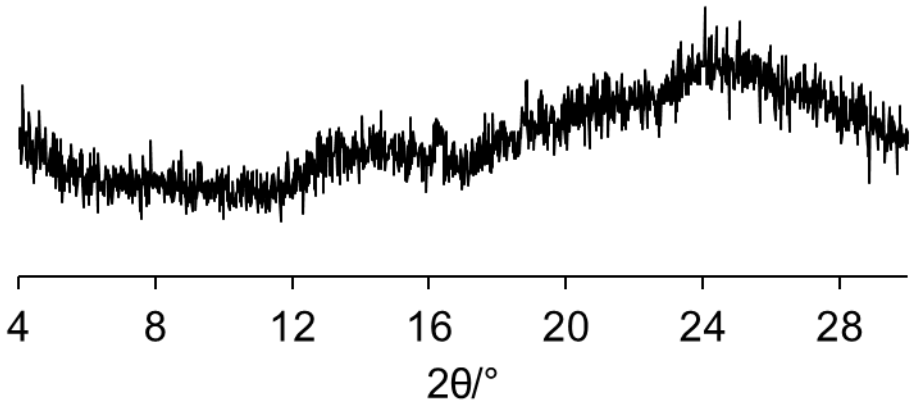

Figure 14 *Amorphous ZnI_2-TPB catenane*

Subsequent *guest exchange* of $CHCl_3$ with xylenes gives an utterly crystalline P-XRD pattern (as seen in ***3.1 Proof of GE***): indeed, molecular guest geometry and host-guest energetic interaction allow *p*X to have a strong templating effect.
Nevertheless, a 4-days immersion of that powder in an equimolar mixture of *o*X, *p*X (2000 μL each one[5]) shows conversely poor selectivity in guest uptake, once the following evidences are taken under consideration.

While the P-XRD pattern remains essentially crystalline (***Figure 15***),

[5] by *Hamilton syringes,* to prevent non-equimolar withdrawals. Indeed, at this stage we are not able to claim whether host-guest chemistry and selectivity are influenced by the relative amounts of solvents in the mixture.

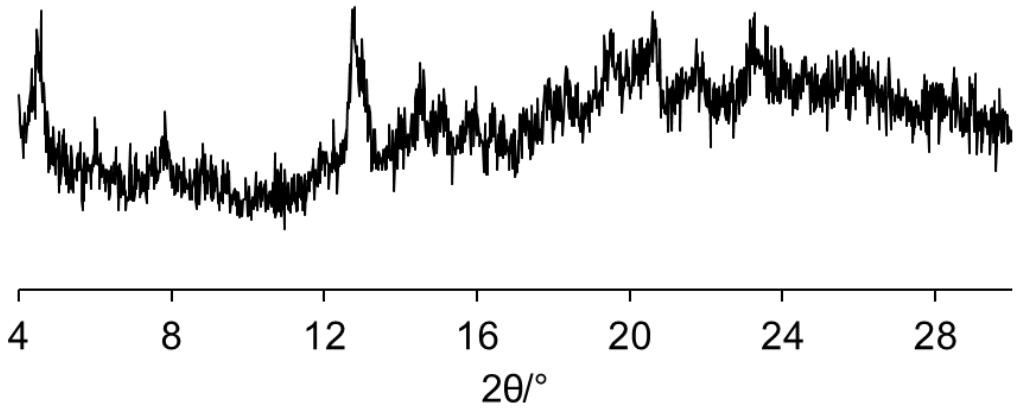

Figure 15 *microcrystals of* $[(ZnI_2)_{12}(TPB)_8]_x(pX)_y(oX)$

focusing on H^1-NMR spectra it is possible to highlight the relative ratio between the two guests inside the cages[6]. To find out selectivities, both supernatant liquid and soaked powder of the abovementioned GE experiment can be analyzed. Unsurprisingly, the former shows no selectivity at all (***Figure 16***) due to the very small quantities under consideration[7]. Unfortunately, the latter detects a quite poor selectivity, around 0.7 or 0.8 mole ox *p*X per mole of *o*X i.e.

$$0.75 : 1 = pX : oX$$

which means a certain *molecular recognition* inside the cages occurs, but it is likely not enough for application purposes. Amorphous powder of $M_{12}L_8$ therefore behaves differently from their respective single crystals.

Eventually, it is remarkable to notice that due to the low reliability of NMR technique to detect such order of magnitude of moles, gas chromatography-mass spectrometry (GC-MS) will be welcome to validate these conclusions.

---

[6] as the ratio between integrals of the peaks associated to *p*X and *o*X (around 2.2-2.3 ppm). By definition, relative ratio is nothing but the selectivity towards xylenes. This discover turned out to be extremely useful at this level of investigation.

[7] Considering the brute formula $[(M_{12}L_8)]_{12}(pX)$ found in **Chapter 3.1** , 100 mg of amorphous catenane contains $12 \cdot \frac{W_{pX}}{W_{M_{12}L_8}} m_{catenane} \sim 20\ mg$ of *p*X. This means that at most ~23 μL of mixture is supposed to enter. This amount cannot be effectively revealed neither as "missing supernatant solvent" from the initial 4 mL solution.

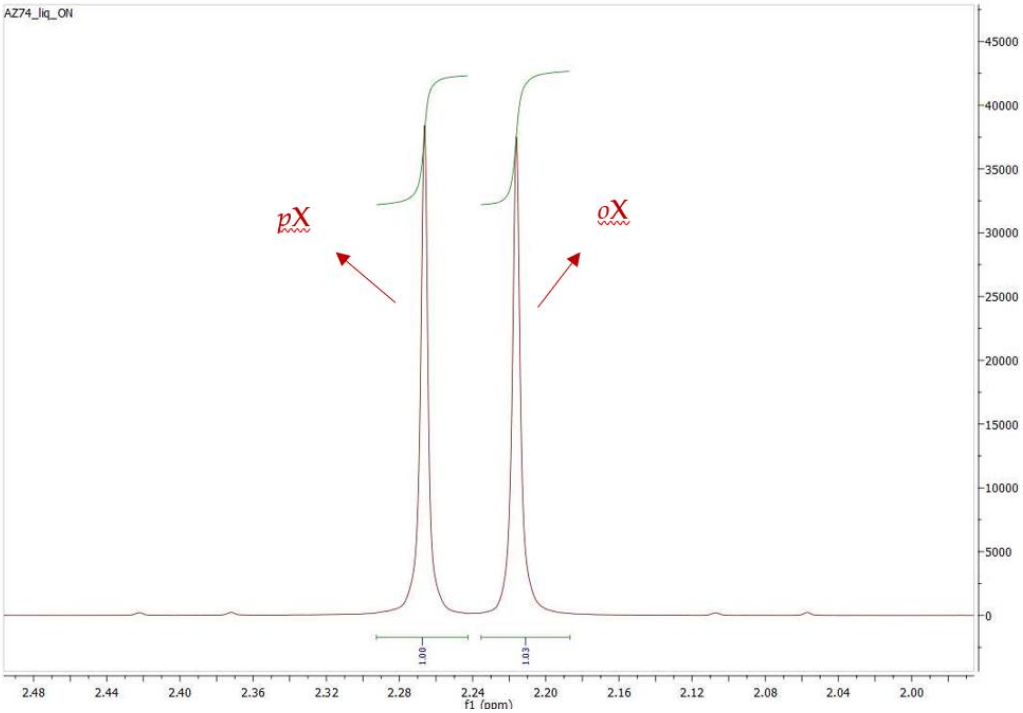

Figure 16 *H-NMR of the supernatant xylenes mixture of an amorphous catenane (a detail)*

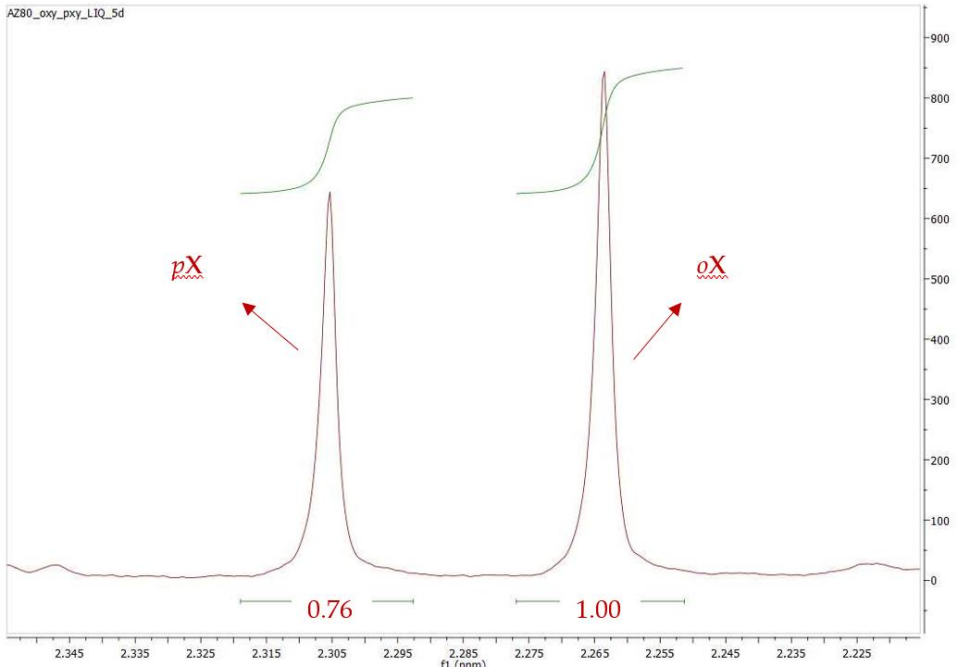

Figure 17 *H-NMR of the amorphous catenane soaked in xylenes mixture (a detail)*

Selectivity of crystalline powder towards isomers

Is there a difference if the starting material is crystalline rather than amorphous? Microcrystalline powder of ZnI_2-TPB catenanes can be readily synthesized through *instant synthesis* in *o*-DCB, the strongest templating agent known so far. Once stated the crystallographic nature by P-XRD (***Figure 18***):

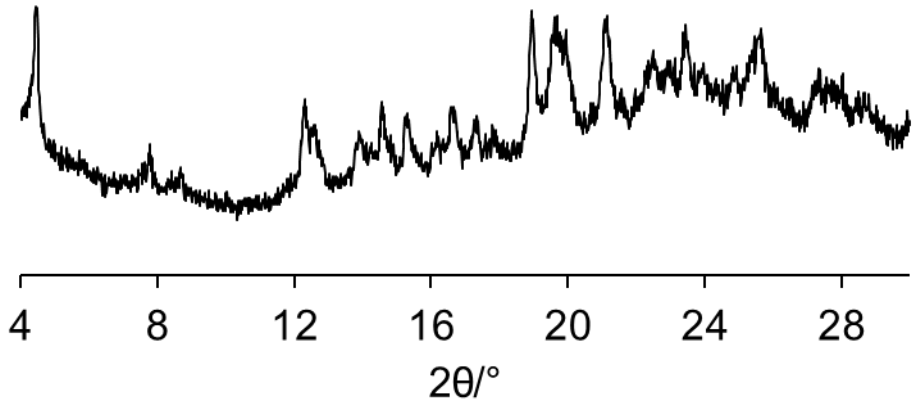

Figure 18 *micrcrystalline powder of* $M_{12}L_8G_6$

A 4-days immersion of that powder in an equimolar mixture of *o*X, *p*X (2000 μL each one) outlines poor selectivity in isomer trapping (***Figure 19***), in perfect accordance to the previous case.

Additionally, considering the dynamic behaviour of poly-[*n*]-catenanes [4], these selectivity experiments in batch styles were carried out with and without methanol as *templating agent*, to check whether the responsiveness of our material is influenced by swelling ability and/or shrinkage of the microcrystals of icosahedral nanocages. Nonetheless, no remarkable differences emerged.

In conclusion, despite the self-evident single crystal selectivity, once powders are soaked in liquid guests the behaviour is clearly different.

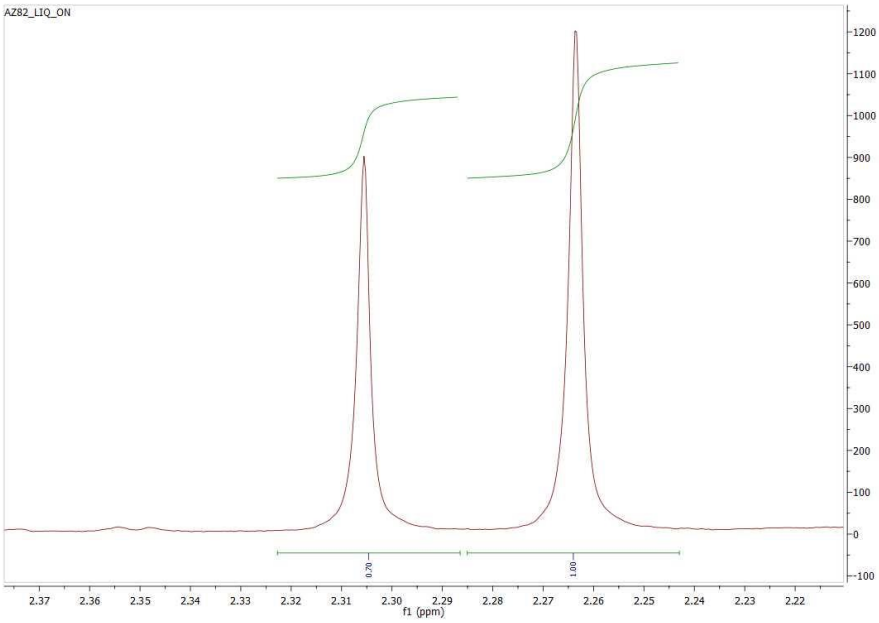

Figure 19 *Microcystalline powder soaked with xylenes mixturs shows a light selectivity towards isomers*

Powder selectivity towards other petrochemical species.

Furthermore, experiments in powder form amongst mixtures of xylenes and ethylbenzene (another petrochemical cut-off, ubiquitous with xylenes), cyclohexane and benzene have been set up.

A number of experiments were done with ethylbenzene (hereafter, EB) to characterize it fulfilling its degrees of freedom in catenane formation: both GI and GE with EB are performed in ZnI_2-TPB poly-[*n*]-catenanes, which are in turn synthetized via *neat grinding* or *instant synthesis*, for 24h and 48h of soaking of powders (100 mg) in EB (**Figure 20**). Essentially, EB appears to be a weak templating agent and (reasonably) the longer the system soaks, the more crystalline the P-XRD pattern becomes.

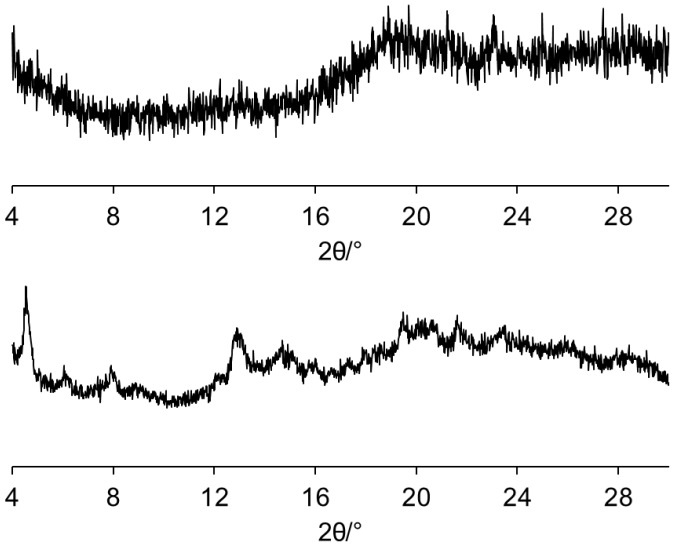

Figure 20 *EB experiments. 24h-GI (up) and 48h-GI (down)*

Now, if *p*X easily enter the cages and EB does not, what will be the result of a mixture soaking? Unfortunately, a *neat grinding* of ZnI_2-TPB followed by overnight *guest inclusion* of equimolar mixture of *p*X and EB detects not only an absence of the expected sharp selectivity (at most, 1 : 0 = *p*X : EB) according to the "molecular sieve" effect (*Application: an engineering perspective*), but seems even that the presence of EB hinder the "natural" templating ability of *p*X (***Figure 21***).

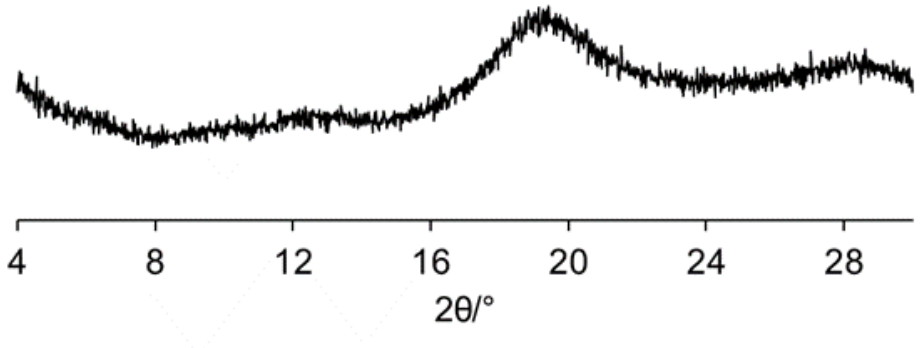

Figure 21 *selectivity experiment between pX and EB. While the presence of only pX produce a crystal pattern, the addition of EB hinder the pX entrance.*

Another candidate was cyclohexane (CE), chemically quite similar to the previous species, while the main difference consists of the absence of aromatic ring, hence a lack of π–π stacking interactions. This difference is crucial, above all, since catenane could

not be even formed by *instant synthesis* – CE is unable to solubilize the ligand. Therefore, *neat grinding* coupled with *guest inclusion* was perfomed. The PXRD pattern remains amorphous (***Figure 22***), hence the guest does not enter. Subsequent selectivity experiments does not yield relevant results.

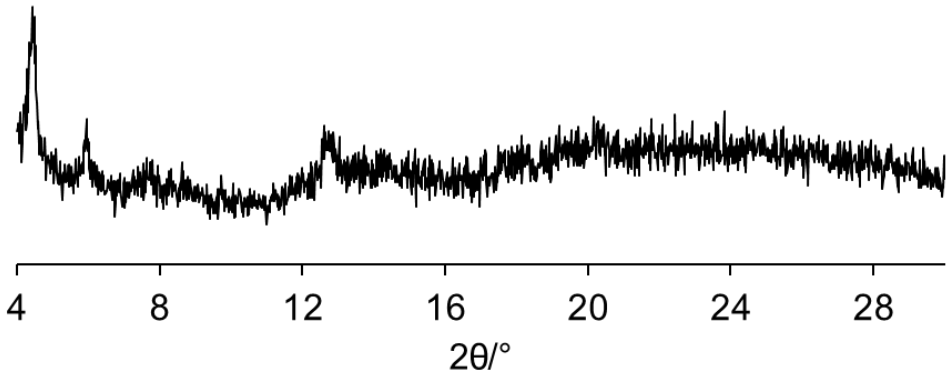

Figure 22 *neat grinding and guest inclusion with cyclohexane.*

Possibly, either in the case of EB or CE, the worse ability or *p*X to enter can be explained either as a "**masking effect**" of the foreign liquid which hamper the guest to enter (EB and CE "mask" the pores to *p*X) or a "**washing effect**" can occur (an initial trapping of *p*X might be counterbalanced by a following flow of EB which, even though does not enter the cages, partially "wash away" the embedded *p*X [4,5]

These preliminary evidences and the toxicity of benzene led to the decision to not deepen the analyses to the behaviour of benzene and other species.

Overall, this lack of proper molecular recognition (even among xylene isomers) together with the *Proof of the G.E.* presented at the beginning of the previous chapter – wherein powder $M_{12}L_8(pX)_{12}$ undergoes *guest exchange* with *o*-DCB, despite later analysis shows that crystals have opposite preferential molecular recognitions – indicates that the powder investigation unfortunately fails in the purpose of finding out strong isolation abilities among isomers and pollutants.

Plug-flow approach. Catenanes as molecular sieves. Adsorption columns

Last chance consisted in looking at similarities between interlocked cages and industrial adsorbent beds: this has prompted the concept of exploiting the molecular recognition property to remove small traces of liquid contaminants. Essentially, the goal was to understand if it is possible to purify a liquid flow contaminated by

aromatic species (such as NB), bypassessing the liquid through a packed powder of catenanes

Hence, a glass-made Pasteur pipette has been fixed vertically and filled with 100 mg of ZnI_2-TPB catenane, properly packed, to simulate a *plug-flow reactor* or a chromatographic column (see ***Figure 23***).

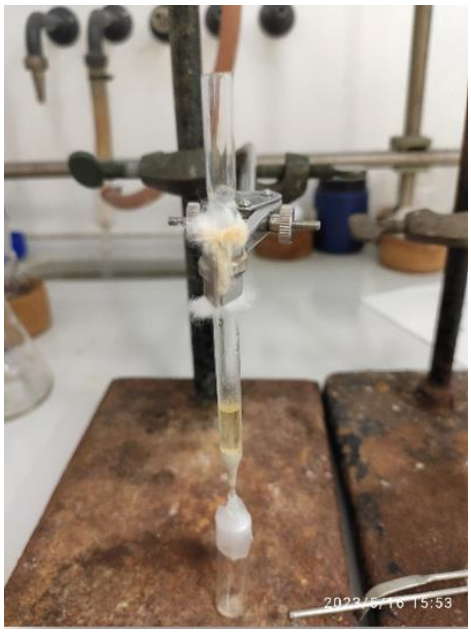

Figure 23 *Picture of a rough 'adsorption column': a glass-made Pasteur pipette filled with catenane in powder form*

In this context, 100 mg of catenane in powder form was carefully packed into the pipette. Then, 2 mL of chloroform and 2 mL of methanol were poured in the pipette both to 'wash the powder' from unreacted reactants and to pack more finely the *adsorption bed* (to homogenize the bed and limit the transport phenomena). Once the washing liquid was completely percolated (depending on the experiment, from few tens of minutes to some hour), the pipette was filled with a 2.02 mL of chloroformic NB mixture[8] (20 : 2000 = NB : $CHCl_3$). Once all the liquid is passed through and collected in a vial below, the solid is left to get dry and both parts analyzed (through P-XRD and/or NMR). Changing the degrees of freedom (whether to pre-washing or not, with or without external pressure, one or two columns in series, amorphous or microcrystalline powder as a packed bed, powder bed height i.e. residence time), no remarkable results were recorded.

[8] In perfect analogy with what done before, to compute the maximum, expected guest uptake, consider the brute formula $[(M_{12}L_8)]_6(NB)$ found in **Chapter 3.1**. 100 mg of amorphous catenane ~ 20 *mL* of *NB*

For the sake of exemplification, a chloroformic NB mixture, passed through two atmospheric pressure, previously washed, amorphous, packed columns, still contains ca. 14 of initial 20 µL of NB[9] (***Figure 24***). So, the great majority of "contaminant" still passes the adsorption bed. Again, further work will consist in verifying these findings with GC-MS analyses, once the poor consistency of this kind of analysis is considered[10].

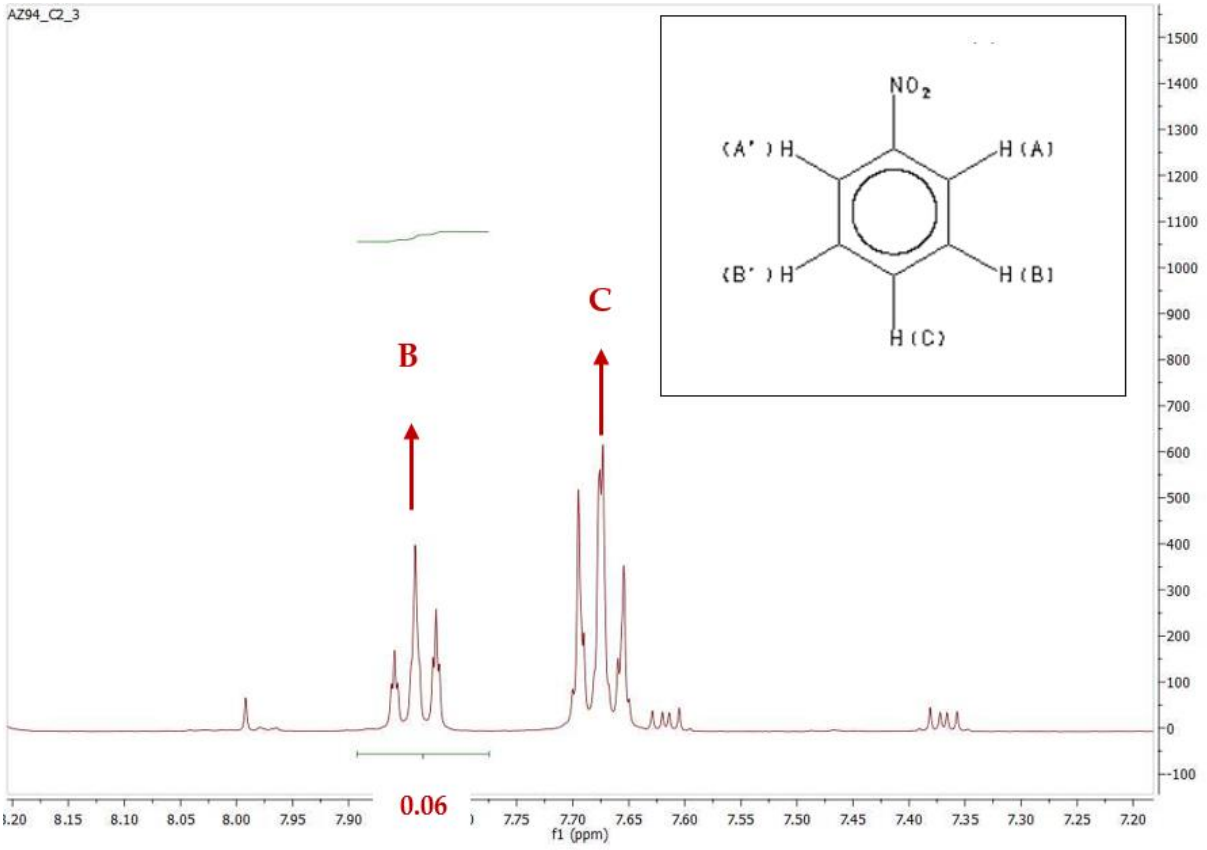

Figure 24 *H-NMR of the outlet, "contaminated stream" of chloroform (a detail).*

[9] Having a 50 µL internal standard of acetonitrile in $CDCl_3$ 1:9 Having a 10 µL internal standard of acetonitrile:$CDCl_3$=1: 9 means that 1 µL of reference is inside the NMR tube. Then, 50 µL of sample gives a peak integral of 0.06 times the one of acetonitrile (in hydrogen-B). Hence, considering multiplicities, densities, molar weights the overall NB remained in the outlet stream is $\frac{0.06}{1/3} \cdot 1\ [\mu L\ ACN] \cdot \frac{0.786\left[\frac{mg}{\mu L}\right]}{41{,}05\left[\frac{mg}{mmol}\right]} \cdot \frac{123{,}11\left[\frac{mg}{mmol}\right]}{1200\left[\frac{mg}{\mu L}\right]} \sim$ 14 µL of the initial 20 µL.

[10] Indeed, considering the very small quantities under consideration, the very small volumes to withdraw and sensibilities of lab tools , if the integral was 0.05 instead of 0.06 (which is anyway a mistake of 20%) it would lead to 12 µL passed

3.3. Synthesis and characterization of a new ligand

In fact, this part of the work is the functionalization of TPB by adding three methyl groups by keeping the symmetry of the ligand which was already started in the group but the aim here was to optimize the synthetic procedure to increase yields and reducing the synthesis time.

The driving force behind this idea was the following. Because the ligand plays a crucial role in the self-assembly of $M_{12}L_8$ poly-[*n*]-catenanes by coordinating with metal ions and by directing the overall spatial arrangement, how small variations in the chemical structure of the ligand can affect the formation of the $M_{12}L_8$ poly-[*n*]-catenanes? Does a functionalized TPB give the 1D chains of interlocked icosahedral cages as well using the various crystallization approaches used so far?

Identification, chemical synthesis and work-up

In this context, the first idea has been to identify possible ligands prepared through functionalization of commercial TPB. Possible species could be the ones shown in ***Figure 25*** X

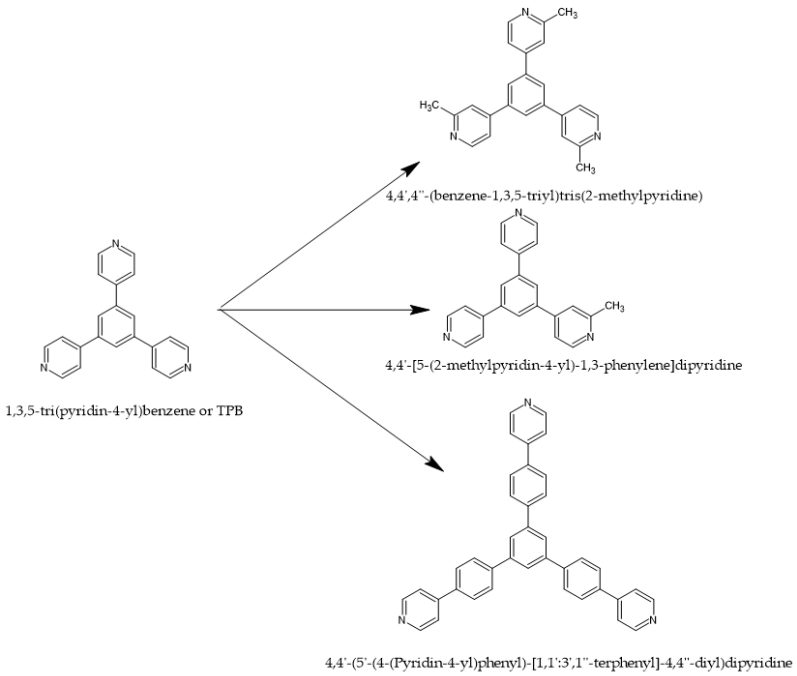

Figure 25 *Diversification of the ligand. Possible candidates*

The functionalization consists, respectively, in the symmetric methylation of standard TPB in the outer pyridinic ring, in a single methylation or in a radical increase in the overall ligand size. Further candidates can be found in the diagram shown below. Since the first structure (from hereafter *mTPB*) was already synthesized but its behaviour was not fully exploited yet, it has been decided to continue focusing on such synthesis.

Previous work identified 4,4'-(5-bromo-1,3-phenylene)dipyridine (hereafter labelled as *mTPB*) and the selected chemical path consisted of the so-called *Suzuki-Miyaura Coupling*.[51]
That is, indeed, one of the most widespread classes of reactions to create carbon-carbon bonds. It involves the reaction of an aryl boronic ester with an aryl halide, catalyzed by palladium species in alkaline environment (*e.g.* KOH (aq)), as exemplified in ***Figure 26***:

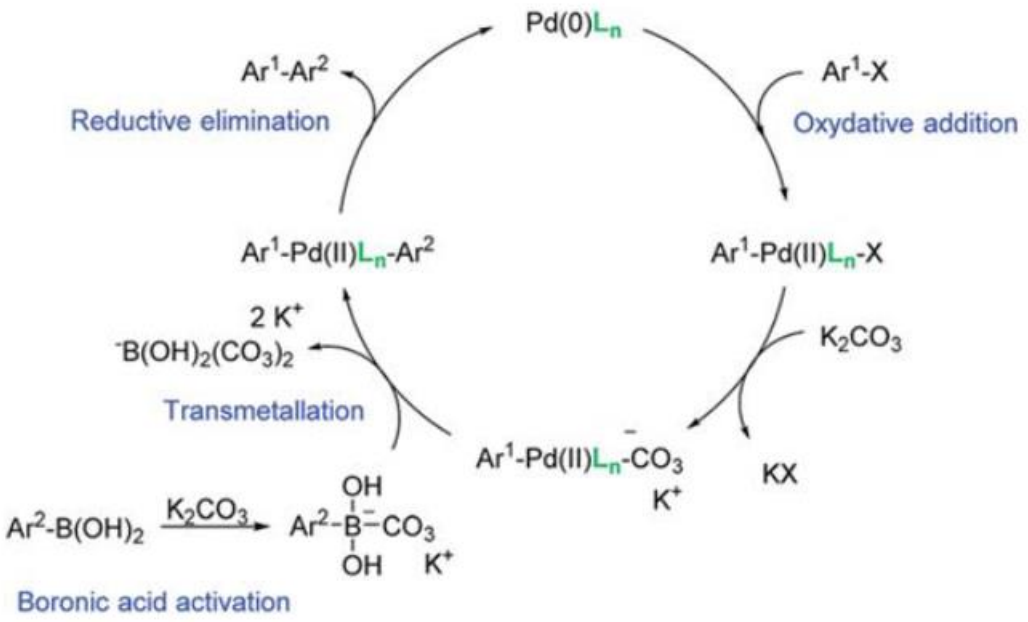

Figure 26 *Catalytic cycle of Suzuki-Miyaura Coupling*

From a chemical point of view, the entire process is a catalytic cycle in which the $Pd^{(0)}$ species is oxidised to Pd(II) and an intermediate with the aryl halide is formed. This intermediate is formed more or less easily depending on the strength of the Ar-X bond, following the trend

Ar-I > Ar-Br > Ar-OTf >> Ar-Cl ~ ArOTs.

The aryl boronic ester then participates, creating an Ar-Pd-Ar' intermediate. Finally, the C-C bond is created through a reductive elimination reaction, yielding Ar-Ar' and regenerating the catalytically active Pd(0) species. The presence of a base is required for boronic acid activation via the production of the matching "ATE" species.

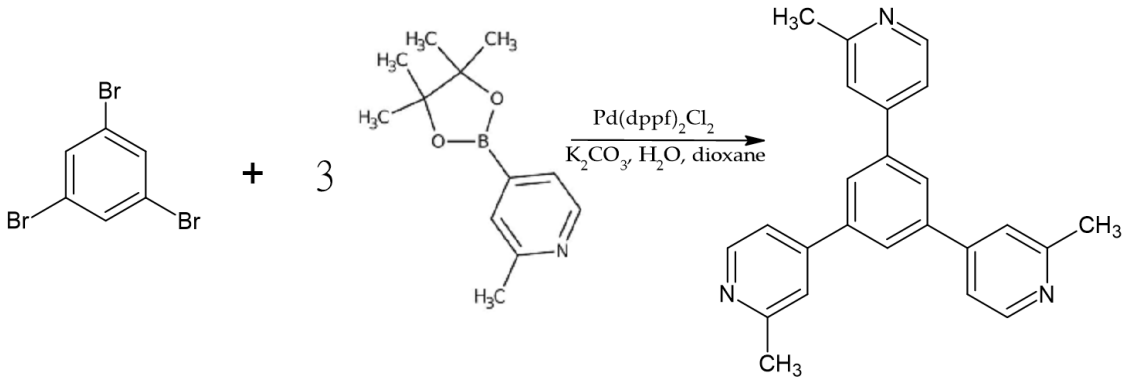

3-Br Benzene 2-met-Pyr-Boronic esther mTPB

From a pragmatic point of view, it is notable just that the process consisted in a 24-hour, round-bottom flask reaction in organic-aqueous solution, heated at 110°C, where vigorous stirring and reflux condenser are guaranteed. Details about reaction and technical aspects are provided in the dedicated section (*Materials and Methods*).

Whilst the extent of reaction can be checked by thin-layer chromatography (consider that reaction goes to completion since the aromatic ring and Suzuki-Miyaura Coupling provide an autocatalytic reaction), work-up consists in liquid-chromatography purification (*either isocratic or gradient mode*), liquid-liquid extraction and final product drying.

Ligand Characterization

Once synthesized the mTPB, the subsequent step consisted in its characterization, either through typical solid-state techniques (i.e. powder and single crystal X-Ray Diffraction) and through common analytic chemistry techniques (i.e. Mass Spectroscopy, IR, NMR etc).

First, the raw white powder solid was purified, dried, and analyzed by PXRD analysis, showing ecellent crystallinity as shown in ***Figure 27***:

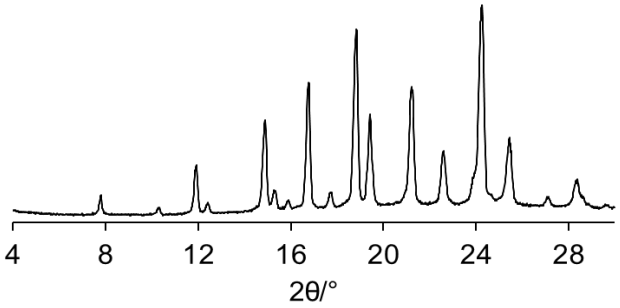

Figure 27 *P-XRD of mTPB*

As shown in Figure 26, the observed Bragg peaks are very sharp and whose overall pattern completely matches with the PXRD of a previous mTPB, thus, it is therefore the desired compound.

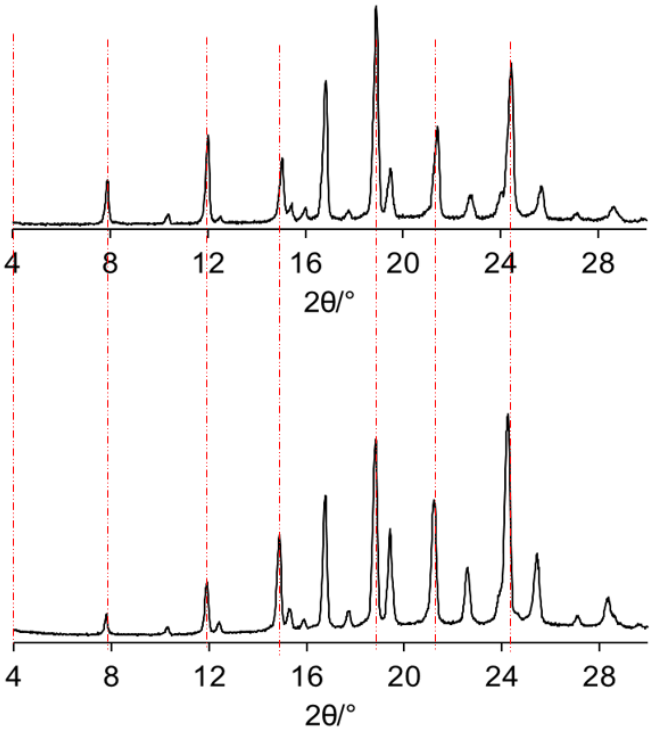

Figure 28 *P-XRD comparison with a previously synthesized mTPB*

Additionally, a higher level of X-ray diffraction is represented by the SC-XRD (see the dedicated chapters in *Introduction* and *Material and methods*). In order to carry it out it is necessary to produce large, single crystals: therefore, a recrystallization of the previous powder must be performed. Generally speaking, the slower the

crystallization is, the larger the crystals will be; the most suitable solvent seems to be chloroform or dichloromethane (DCM). In practice, mTPB is dissolved in DCM in a round bottomed flask, and then left vaporized through a rotary evaporator. The formed crystals are analyzed with the SC-XRD at 173 K, providing us four levels of information.
Firstly, from the SC-XRD experiments, the crystal structure shows the successful synthesis of mTPB (***Figure 29***):

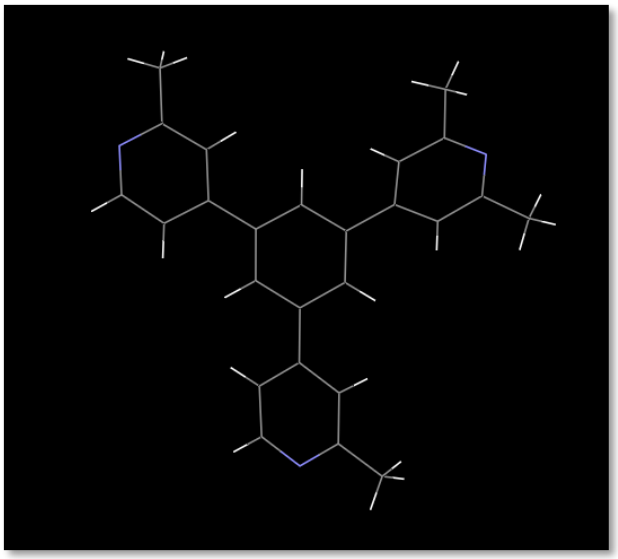

Figure 29 *SC-XRD structure*

Interestingly, in this case one of the aromatic rings exhibits a methyl group in excess which can be due to the rotational nature of the σ-bond between benzenic and pyridinic rings.

Afterwards, it is possible to deepen the analysis looking for the whole **Unit cell** of the crystal, in order to understand the molecule's surroundings and its packing abilities, quite interesting in a crystal engineering perspective.
Ligand mTPB crystallizes in a *monoclinic lattice* with the body-centered space group **I 2/a**, whose lattice parameters are:

$$a = 7.76272(16)\ \text{Å},\ b = 16.6743(4)\ \text{Å};\ c = 14.8409(3)\ \text{Å}$$

$$\alpha = 90°,\ \beta = 103.9°,\ \gamma = 90°$$

and total volume V = 1864,53 $Å^3$.

In the picture below (***Figure 30***), the *a*, *b* ,*c* axis are respectively the red, green and blue ones.

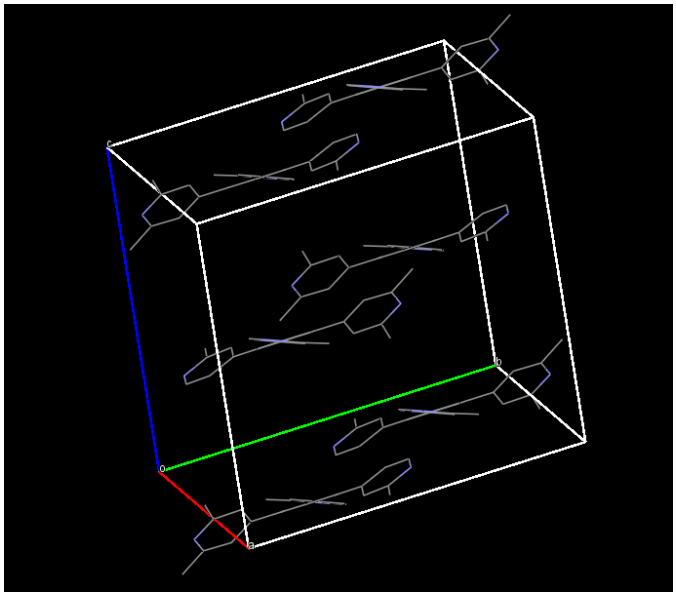

Figure 30 *mTPB: a unit cell.*

Moreover, within the unit cell, the asymmetric unit consists of 1.5 pyridinic rings (of 3 totally) and half of the central benzene ring. From an angular point of view, the central benzene ring and one of the pyridine rings are perfectly co-planar (180°), while the other two pyridines are nearly co-planar (179.26°).

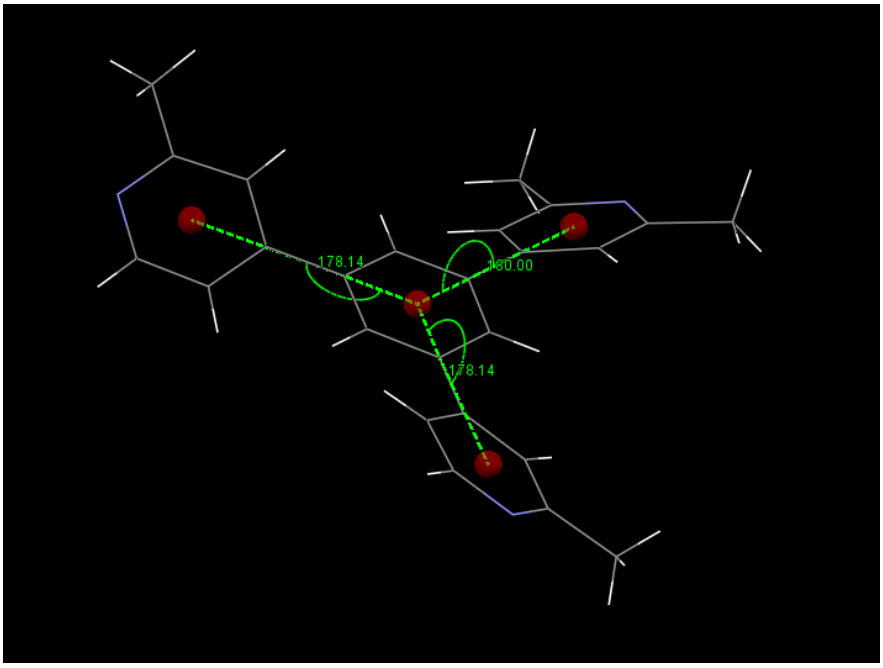

Figure 31 *mTPB: angles described by aromatic rings within the same molecule*

Additionally, in the lattice the mTPB molecules are held together by means of two $C_{methyl}\cdots C_{pyridine}$ ($d_{C\cdots C}$ = 3.228 Å or 3.139 Å) short contact interactions between the a -CH_3 belonging to a first mTPB molecule and two adjacent C of a pyridine ring of another close mTPB. Also the two of three methyl-H of the first mTPB interact with the two adjacent $C_{pyridine}$, while the third H interacts with one of the $C_{benzene}$ of another mTPB molecule, opposite to the second mTPB.

The short intermolecular contacts described result in planar layers of mTPB molecules expanding along the crystallographic b-axis and c-axis; those planar layers are held together by means of π-π interactions established between the central benzene rings and the external pyridine rings (dbz···py =7.421 Å, see ***Figure 32***). As a result of such interactions the layers of TPB are expanding along the c-axis resulting in a closely packed structure (d = 2.461 g/cm^3).

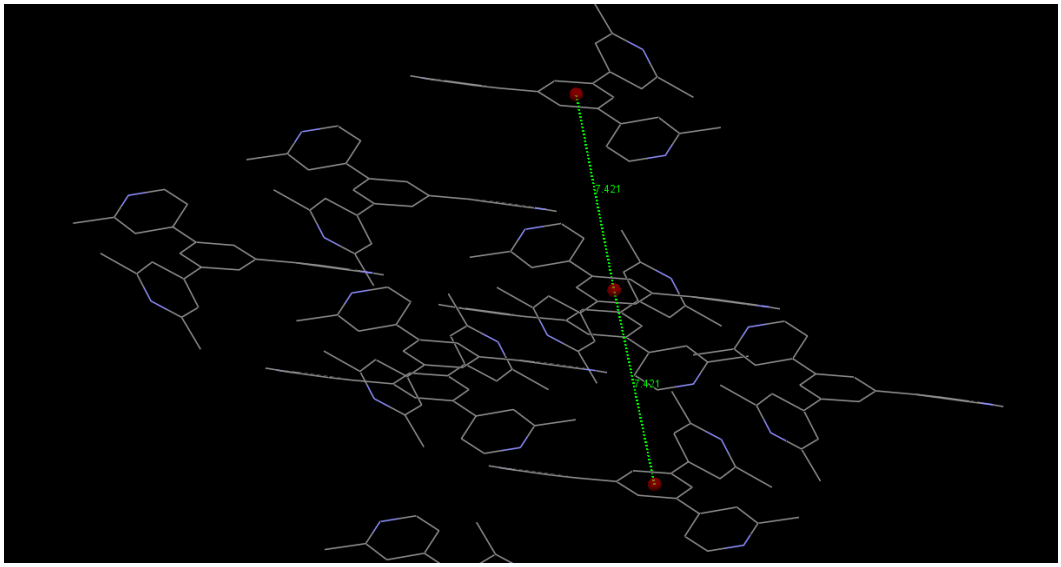

Figure 32 *mTPB: planar layers and rings distance*

Further analyses via H^1-NMR, IR Spectrophotometry and Mass Spectroscopy confirms that the whte solid produced in the synthesis corresponds to m-TPB. NMR pattern is the following and it is compatible with mTPB:

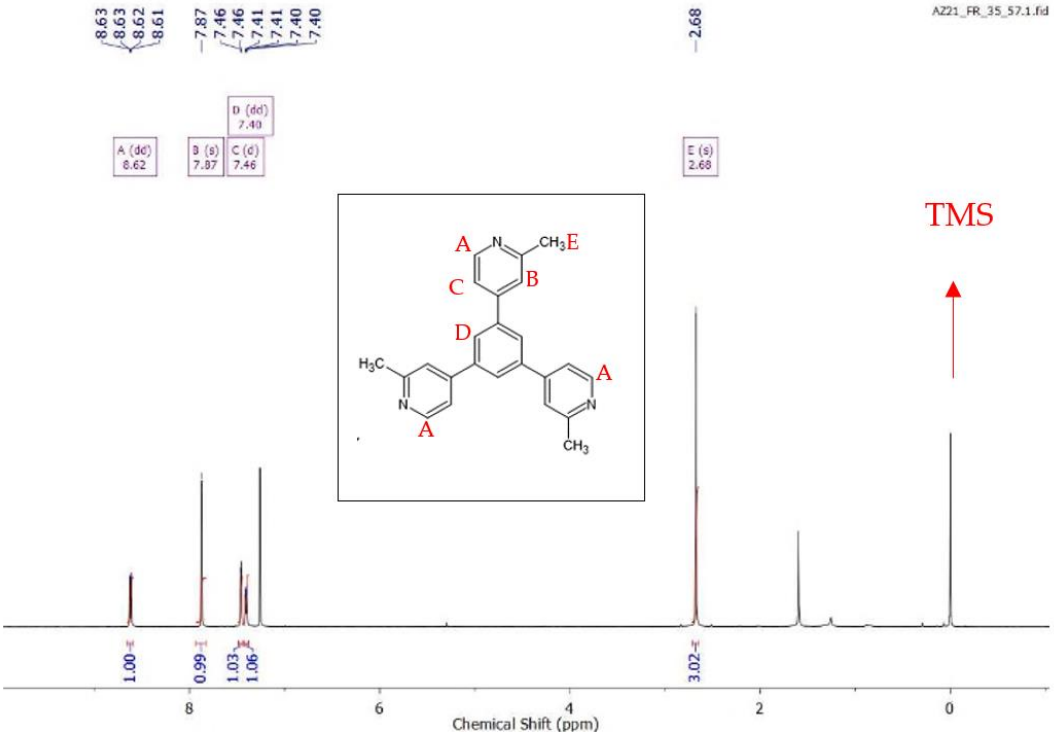

Figure 33 *NMR analysis of mTPB*

Here the peak at 0 is the TMS, one of the most common internal standards; more interesting are the five peaks associated with the *five H atom classes* in the molecule: from right to left according to the electron deficiency, singlet or doublet according to "*hydrogen in alpha*" population and multiplicity of 3 for each one (except for methyl E, which have a multiplicity of 9). Eventually, the fact that this pattern coincides with previous syntheses of the ligand crowns the evidence that NMR have successfully detected the mTPB.

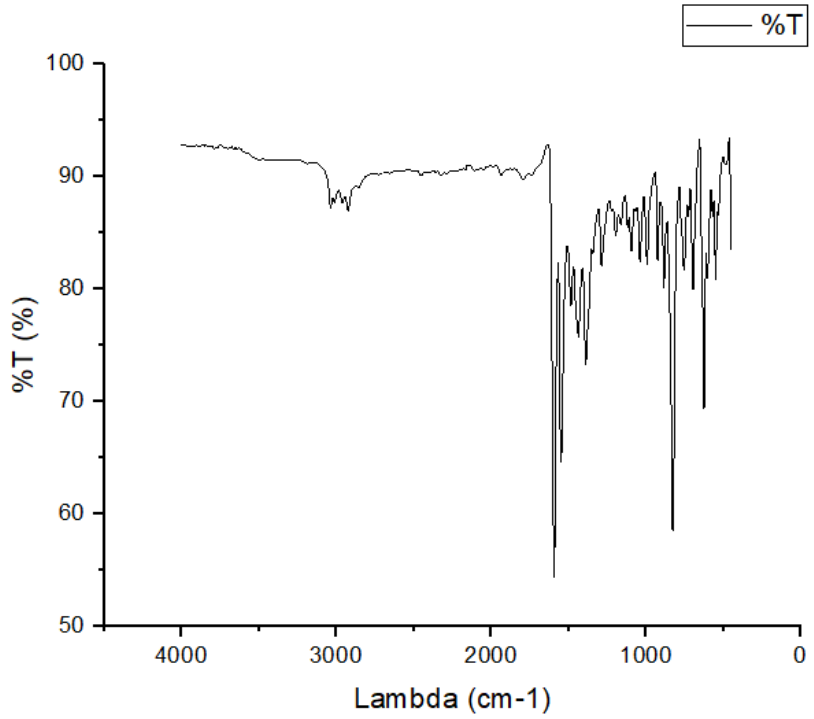

Figure 34 *IR analysis of mTPB*

For what concern IR Spectrophotometry, the pattern matches with the analyses of previously synthesized ligands and, regarding Mass Spectroscopy, since the mass weight of mTPB is 351 g/mol – indeed the most intense peaks – while the 254 one represents a break down of the molecule in the most likely position – i.e. pyridine-benzene σ-bond.

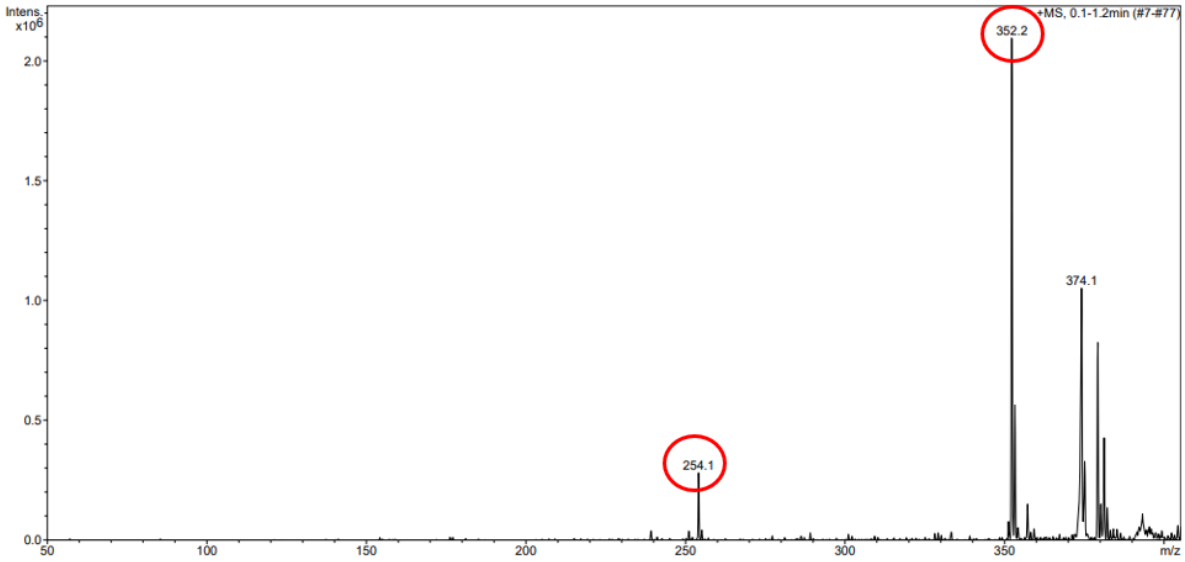

Figure 35 *MS analysis of mTPB*

Optimization attempts

After several batches, it has been incidentally noticed the overall yield is always still around 50% wt. Either from an engineering point of view (i.e. seeking for the efficiency, in a scale-up perspective) and from a sustainable outlook (i.e. consider previous studies about green chemistry), we wonder whether it is possible to increase the synthesis yield.

Multiple attempts have been carried out, from an optimization in the downstream purification (i.e. performing the liquid chromatography in a *gradient mode*, instead of an *isocratic one*) to an unsuccessful *microwave variant*, passing through the change in operating conditions (time and temperature). Gradient-LC was found to roughly halve solvent exploitation.

From the point of view of the yield, since it remained roughly constant despite our strives, apparently the yield does not depend on the effectiveness of work-up. It has also been observed that authors' declared conversion is higher as well as authors' quantities are much smaller: thus the idea to resize the reaction by reducing the reactant quantities closer to one declared by the recipe (from 1000 mg to 50 mg of stoichiometric product, whereas the recipe was calibrated for ca. 70 mg) was implemented, leading to a yield burst to ca. 80%.
Thus, a +60% enhance has been finally achieved.

3.4. On the application of the new ligand within Catenanes formation

Once demonstrated a new ligand is quite readily synthesizable in a very high degree of purity, it is possible to study its behaviour in interlocked MOCs formation.
Generally speaking, a poly-[*n*]-catenane self-assembles along three paths (see *Methods: synthesis of Catenanes and ligands*) and according to three degrees of freedom (i.e. the ligand, the metal salt, the guest). Thus, the influence and the behaviour of the functionalized ligand will be presented and analyzed, by fixing the first and the second degree of freedom (i.e. mTPB is the ligand, $ZnBr_2$ is the metal) while varying the third.

Kinetic amorphous powder

The first way to synthesize poly-[*n*]-catenanes is via *neat grinding* of TPB and ZnX_2. As seen, this is a solvent-free technique which leads to amorphous powder of a metastable product through kinetic control.

Grinding of mTPB and $ZnBr_2$ for 30-60 mins gives amorphous powder (***Figure 36***). Despite it is not possible to discern whether it is a catenane, however by comparing the P-XRD pattern of $ZnBr_2$-TPB with the one of $ZnBr_2$-mTPB it is possible to guess similarities in crystallinity (at least, in a short-range order). Please, notice that even if the two patterns coincides, it does not mean that they are the same compound. Interestingly, the two diffractograms actually match significantly (***Figure 37***).

Furthermore, by *guest inclusion* in *o*-DCB it is possible to infer the host-guest chemistry of the synthesized material. A crystalline diffractogram is achieved (***Figure 38***): guest uptake and templating effect occur involving a structural reorganization.

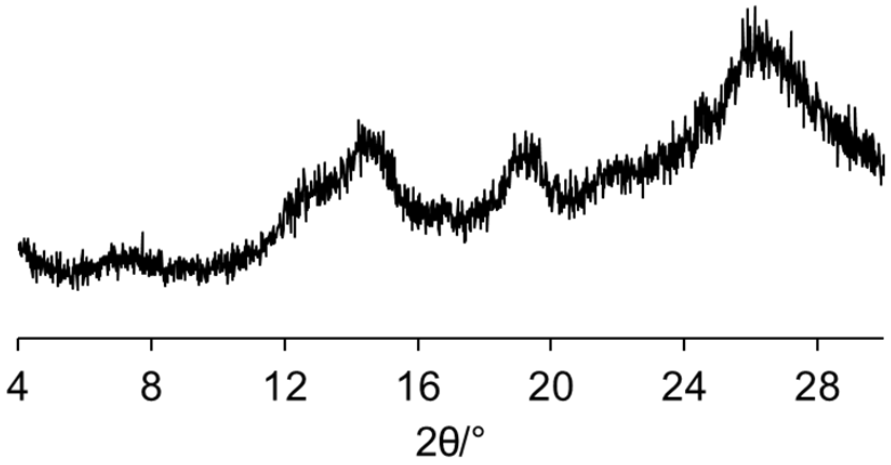

z

Figure 36 *neat grinding of mTPB, $ZnBr_2$*

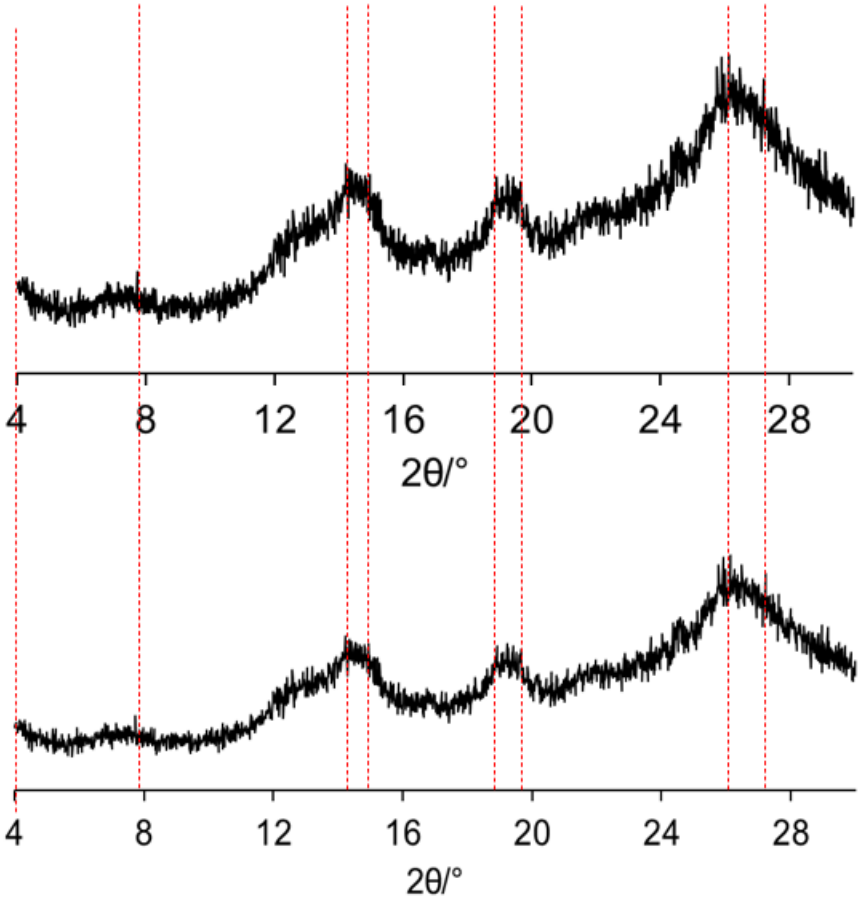

Figure 37 *comparison between TPB+$ZnBr_2$ (up) vs mTPB+$ZnBr_2$ (below).*

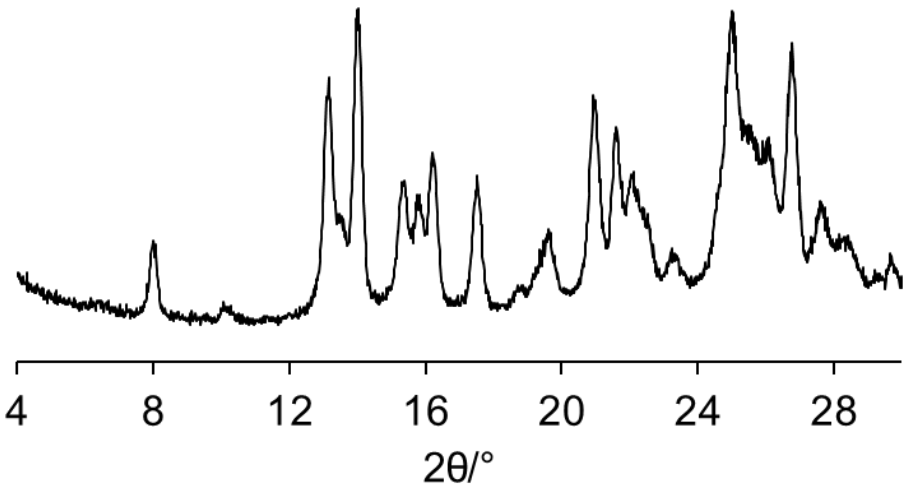

Figure 38 *Guest inclusion of the amorphous powder in o-DCB leads to mycrocrystals*

Kinetic crystalline powder

The second way to synthesize poly-[*n*]-catenanes is via *instant synthesis* of TPB and ZnX_2 in a templating solvent. As seen, this is fast crystallization technique which leads to microcrystalline powder of a metastable product through kinetic control.

The addition of a a methanolic solution of $ZnBr_2$ to an homogeneous solution of mTPB in *o*-DCB gives powder with a sharp P-XRD pattern. Similarly, the comparison with *instant synthesis* of $ZnBr_2$, TPB perfectly matches (***Figure 36***). Furthermore, it is qualitatively the same of previous neat grinding followed by guest inclusion, as expected.

Nevertheless, it is not possible to extract more information from PXRD data. To disclose the crystallographic nature of these MOFs, further analysis by *electron diffraction* will be required.

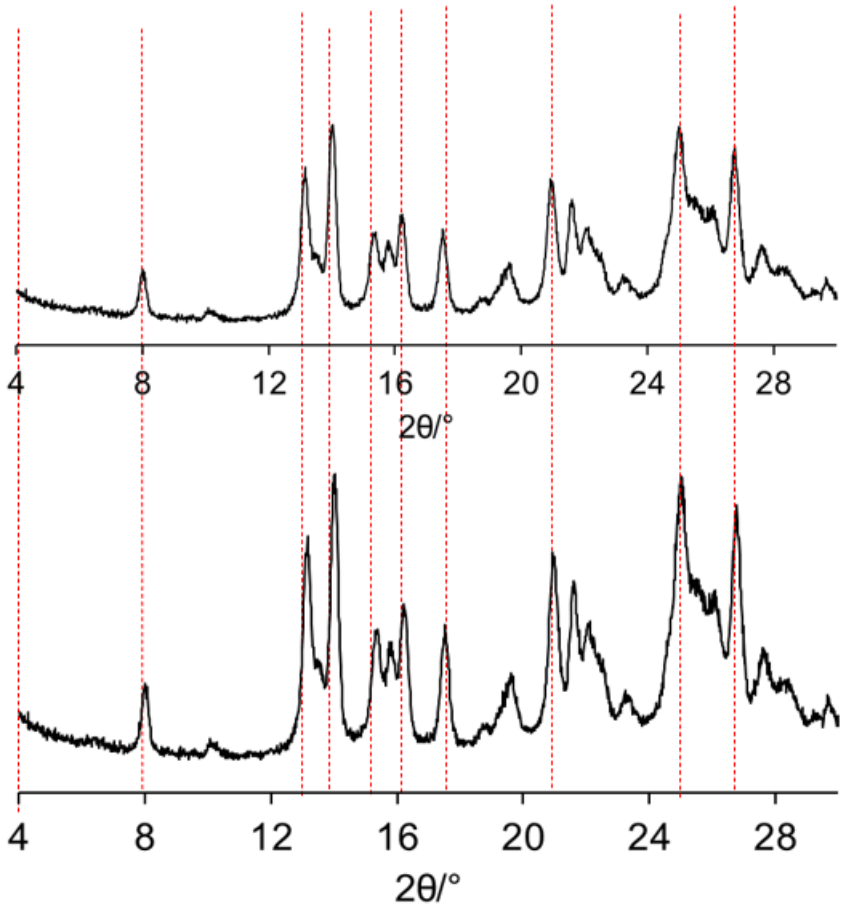

Figure 39 *comparison between TPB+ZnBr2 (up) vs mTPB+ZnBr2 (below).*

In conclusion, while TPB and the metal salt lead to *interlocked metal-organic cages* as the stablest (thermodynamic) product, mTPB leads to *planar layers of metal-organic frameworks* as stable product.

Thermodynamic single crystals

The second way to synthesize poly-[*n*]-catenanes is via *three-layer method*. As seen, this leads to macro crystals of a stable product through thermodynamic control.

Slow crystallization of mTPB and $ZnBr_2$ in *o*-DCB results in single crystals formation after 1 week, as expected. SC-XRD experiments show the following crystal structure (***Figure 40***):

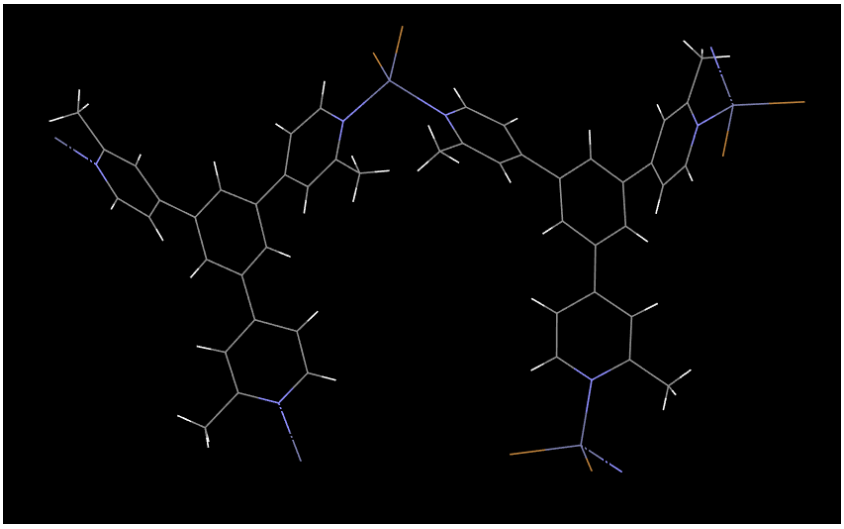

Figure 40 *SC-XRD structure*

In this case, methylation on each pyridinic ring is self-evident and, most remarkable difference to basic TPB is that two ligands are joint together by means of the metal salt.

It is possible to deepen the analysis looking for the whole **Unit cell** of the crystal, to understand the framework's surroundings and its packing abilities, quite interesting in a *crystal engineering perspective*. It reveals a **trigonal system** in the rhombohedral ***R*-3 space group** with the following lattice parameters:

$$a = b = 21.4323(2)\ Å^3,\ c = 19.3803(2)\ Å$$

$$\alpha = 90°,\ \beta = 90°,\ \gamma = 120°\ Å$$

and total volume V = 7709.54 $Å^3$.

In the picture below (***Figure 41***), the a,b,c axis are respectively the red, green and blue ones. By the way, it is possible to appreciate the planar, thick layering of the formed framework. Differently from the resulting structure of $[(ZnI_2)_{12}(TPB)_8]_6$(*o*-DCB), no catenation of nanocages occur, but a simpler bidimensional coordination network (CN).

Within the unit cell, the asymmetric unit consists of 2 pyridinic rings (belonging to two different ligands) one third of the central benzene ring (2 carbons and 1 hydrogen) and 1 zinc salt (which joins the pyridines. Overall, the characteristic width of each layer is about 3-4 Å, while the distance between two adjacent layers is ca. 8-9 Å.

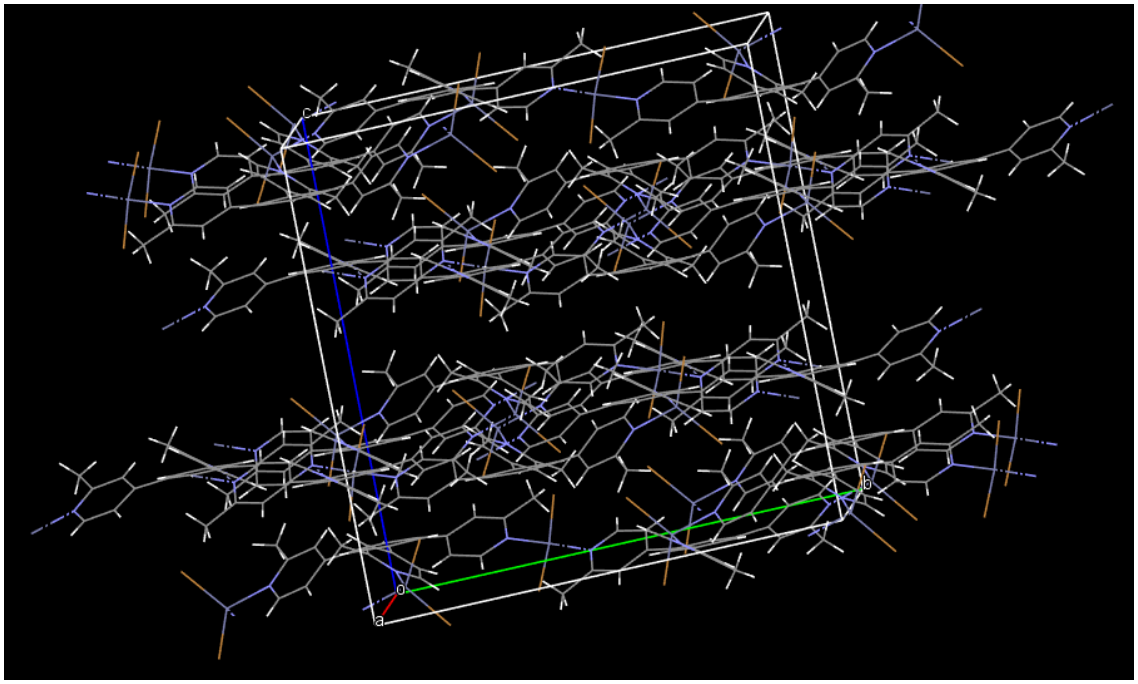

Figure 41 *mTPB: a unit cell, wherein an insight of the 2D Coordination Network can be glimsed.*

Conclusions

Dealing with mTPB and $ZnBr_2$, fast crystallization methods lead to structures and have a behaviour compatible with the corresponding TPB-$ZnBr_2$ structures (i.e. poly-[*n*]-catenanes), both in crystalline and amorphous form. However, experimental information is not enough to claim about their nature: further analyses (e.g. *electron diffraction*) are needed, then.

Slow crystallization, conversely, leads to a dramatic change of structures. Whilst the three layering of $ZnBr_2$ and TPB may give only poly-[*n*]-catenanes or a copresence of catenanes and coordination networks as stable structures (depending on the solvent), mTPB do not form interlocked nanocages at all, giving just CNs as preferential molecules.

Indeed, about the ligands, the use of long ligands generally favours the formation of ultra-large pores and promotes interpenetration rather than frameworks but affects negatively the whole stability favored instead by rigid and compact ligands; for the first time it has been proved that a methylation, instead, utterly hinder the interpretation of 0D cages, preferring instead planar (2D) networks.
Hence, the most relevant claim is that, while the change of the counterion in the metal salt slightly influence the size of crystals and the volumes of the cages due to steric hindrance [52], the change of the ligand drastically change the outcoming structure.

4 CONCLUSIONS AND FURTHER STUDIES

Poly-[*n*]-catenanes show captivating properties,from solvent uptake to molecular recognition, to name a few, have been recently studied thoroughly.
In this context, previous work of the Marti-Rujas research group has consolidated the synthesis routes of these interlocked nanocages, recognised the templating effect and the molecular uptake ability, discovered a viable synthetic pathway for ligand functionalization. Based on it, then, it has been possible to deepen the influence that ligands have within $M_{12}L_8$ nanocages formation, on the one hand, and to broaden their host-guest chemistry knowledge once formed, on the other hand.

Indeed, first of all the molecular separation abilities of ZnI_2-TPB poly-[*n*]-catenanes have been investigated, either in crystal and powder form. Once demonstrated the *guest exchange* property of these $M_{12}L_8$ nanocages, the crystallographic structure of a thermodynamic single crystal – produced via three-layer method with para-xylene as templating solvent – has been obtained by SC-XRD. It was not granted since meta or ortho xylenes, for instance, have difficulties in grow up. The confirmed molecular recognition through π–π binding sites let them be tested for gas-solid reactions, which indeed occurs successfully. Then, consecutive gas-solid guest exchanges with different aromatic vapours were tested, checking whether a preferential molecular separation arises. As confirmed by SC-XRD and DFT, undoubtfully NB is the strongest embedded, preferred to xylenes (*p*X above the others) which are in turn preferred to *o*-DCB. Hence, preferential trapping holds, together with the good affinity of these materials towards paraxylene and nitrobenzene, and a general stability and robustness of the framework over multiple exchange reactions is observed.

Afterwards, attention switched to microcrystalline (i.e. powder) $M_{12}L_8$ nanocages: the exploitation of these interlocked nanocages taking inspiration from some key-applications – notably, isomer separation of petrochemical species (*i.e. xylenes*) or selective adsorption

of pollutant species (*i.e. nitrobenzene*) – has been tested. Namely, despite the selective trap of nitrobenzene by single crystals, a chloroformic solution of NB (simulating a contaminated stream to be purified) is not properly purified once passed through a powder of $M_{12}L_8$ nanocages. Also, despite what found in gas-solid reactions, in a liquid guest inclusion not even a preference towards isomers is evidenced in an equimolar mixture of xylenes (every 4 molecules of *o*X trapped in the powder, 5 molecules of *p*X are trapped too).

Parallelly, once established the behaviour of these materials, an emphasis has been placed on the functionalization of the ligand. Optimization studies have been employed to increase the yield, minimize the solvent usage, avoid reactant losses. In particular, a change in the synthetic conditions by changing (i.e. catalyst, quantities etc.) shows that just the resize of the quantities significantly enhance the yield, while the work-up process manipulation (i.e. exploitation of an automatic, gradient-mode liquid chromatography) has led to a relevant solvent minimization.

Hereafter, a focus has been placed on the influence the methylated ligand has within catenane formation (i.e. $M_{12}L_8$ assembly). Dwelling on Br as counterion and knowing that small changes in the salt slightly changes the cage size, small changes in the ligand dramatically change the outcoming product, instead. A symmetric methylation of pyridinic rings undoubtfully hinders the mechanical interpenetration of MOCs leading to more elementary, planar coordination networks as stable frameworks (thermodynamically-speaking).

Importantly, it must be said that analytical techniques used so far in powder selectivity investigation are not mature yet, an future studies should focus on exploit more sophisticate techniques (such as Gas Chromatography-Mass Spectrometry) to validate conclusions found about selectivity in powder form.

Further work aimed to conduct experiments with different counterions to further clarify the influence of cage size and crystallinity on porosity and selectivity of the methylated trys-pyridpylbenzene ligand, as well as expand the horizon of catenation with more complex, large exotridentate ligands.

Thematic bibliography

For those interested, an essential thematic bibliography for the main issues is provided.

About Catenanes

Stoddart, F. et al. (1994). "Mechanically Interlocked Molecules - Synthesis, Characterization, and Dynamics of a [2]Catenane, a Molecular Shuttle, and a [2]Rotaxane." Journal of the American Chemical Society, 116(1), 364-375.

Sauvage, J. P. et al. (1983). "Transition Metals in a Catenane." Angewandte Chemie International Edition in English, 22(11), 836-838.

Leigh, D. A. et al. (2003). "A Chemically and Mechanically Topologized Molecule." Journal of the American Chemical Society, 125(37), 11156-11161.

Dietrich-Buchecker, C. et al. (1984). "Catenanes and Rotaxanes." Journal of the American Chemical Society, 106(1), 304-306.

Wang, Q. et al. (2011). "Polycatenanes." Chemical Reviews, 112(11), 6067-6105.

Liu, G. et al. (2022). "Polycatenanes: synthesis, characterization, and physical understanding". Chemical Society Reviews.

About catenated MOCs (or Catenanes made of MOCs)

Fujita, M., & Ogura, K. (1996). Supramolecular Self-Assembly of Macrocycles, Catenanes, and Cages through Coordination of Pyridine-Based Ligands to Transition Metals. Bulletin of the Chemical Society of Japan, 69(6), 1471–1482.

Martí-Rujas, J., Elli, S., Sacchetti, A., & Castiglione, F. (2022). Mechanochemical synthesis of mechanical bonds inM12L8poly-[n]-catenanes. Dalton Transactions, 51(1), 53–58.

Lu, J.; Poyraz, A. S.; Zhou, F.; Huang, F.; Cao, L.; Wu, D. Angew. Chem. Int. Ed. 2010, 49 (50), 9809–9812.

Witt, M.; Dehnen, S. J. Am. Chem. Soc. 2011, 133 (25), 9656–9659.

Wu, D.; Xu, B.; Liu, X.; Yin, X.; Lu, J. Angew. Chem. Int. Ed. 2012, 51 (31), 7645–7649.

Li, Z.; Hong, Y. Nat. Commun. 2015, 6 (1), 7579.

Wu, Y.; Li, P.; Zhao, B.; Zhang, L.; Li, H.; Li, G.; Zhao, D. J. Am. Chem. Soc. 2015, 137 (43), 13724–13727.

E.S.M. El-Sayed, D. Yuan, Metal-organic cages (MOCs): From Discrete to Cage-based Extended Architectures, Chem Lett. 49 (2020) 28–53.

About MOFs

Zhou, H. C., Long, J. R., & Yaghi, O. M. (2012). Introduction to metal-organic frameworks. Chemical Reviews, 112(2), 673-674.

Yaghi O. M., G. Li. Introduction to Metal-Organic Frameworks. (2008)

Zhou, H. C., Long, J. R., & Yaghi, O. M. (2012). Introduction to metal-organic frameworks. Chemical Reviews, 112(2), 673-674.

Rowsell, J. L., & Yaghi, O. M. (2006). Metal-organic frameworks: a new class of porous materials. Microporous and Mesoporous Materials, 73(1-2), 3-14.

Yanai, N., Kitagawa, S., & Kondo, M. (2018). Mechanisms and functional properties of porous coordination polymers. Chemical Reviews, 118(9), 4702-4720.

About the SCSC and the CAC Process

Ohmori, O., Kawano, M., & Fujita, M. (2004). Crystal-to-crystal guest exchange of large organic molecules within a 3D coordination network. Journal of the American Chemical Society, 126(50), 16292–16293.

Kitagawa, S., Kitaura, R., & Noro, S. (2004). Functional porous coordination polymers. Angewandte Chemie International Edition, 43(18), 2334-2375.

Abrahams, B. F., Moylan, M., Orchard, S. D., & Robson, R. (2003). Reversible single-crystal-to-single-crystal transformations between herringbone and ladder structures. Angewandte Chemie International Edition, 42(16), 1848-1851.

J. Martí-Rujas, N. Islam, D. Hashizume, F. Izumi, M. Fujita, M. Kawano, Dramatic structural rearrangements in porous coordination networks. J Am Chem Soc. 133 (2011) 5853–5860.

About ZnX_2-TPB $M_{12}L_8$ poly-[*n*]-catenanes

S. Torresi, A. Famulari, J. Martí-Rujas, J. Martí-Rujas, Kinetically Controlled Fast Crystallization of M12L8Poly-[n]-catenanes Using the 2,4,6-Tris(4-pyridyl)benzene Ligand and ZnCl2in an Aromatic Environment, J Am Chem Soc. 142 (2020) 9537–9543.

A. Famulari, J. Martí-Rujas, Host-Guest Chemistry of M 12L 8Poly-[n]-catenanes: Inclusion Process by Switchable "closed-Open" Dynamic Channels, Cryst Growth Des. 22 (2022) 4494–4502.

J. Martí-Rujas, S. Elli, A. Sacchetti, F. Castiglione, Mechanochemical synthesis of mechanical bonds inM12L8poly-[n]-catenanes, Dalton Transactions. 51 (2022) 53–58.

Martí-Rujas, J., Elli, S. & Famulari, A. Kinetic trapping of 2,4,6-tris(4-pyridyl)benzene and ZnI2 into M12L8 poly-[n]-catenanes using solution and solid-state processes. Sci Rep 13, 5605 (2023).

Bibliography

1. Fujita, M., Oguro, D., Miyazawa, M., Oka, H., Yamaguchi, K., and Ogura, K. (1995) Self-assembly of ten molecules into nanometre-sized organic host frameworks. *Nature*, **378** (6556).
2. Marti-rujas, A.J., Elli, S., and Zanotti, A. (2023) Supporting information. Molecular Recognition of Aromatics in Spherical Nanocages. *Chemistry - A European Journal*.
3. Marti-rujas, A.J., Elli, S., and Zanotti, A. (2023) Molecular Recognition of Aromatics in Spherical Nanocages. *Chemistry - A European Journal*, **13** (3), 287–288.
4. Famulari, A., and Martí-Rujas, J. (2022) Host-Guest Chemistry of M 12L 8Poly-[n]-catenanes: Inclusion Process by Switchable "closed-Open" Dynamic Channels. *Cryst Growth Des*, **22** (7), 4494–4502.
5. Martí-Rujas, J., Elli, S., Sacchetti, A., and Castiglione, F. (2022) Mechanochemical synthesis of mechanical bonds inM12L8poly-[n]-catenanes. *Dalton Transactions*, **51** (1), 53–58.
6. Chen, Q., Jiang, F., Yuan, D., Chen, L., Lyu, G., and Hong, M. (2013) Anion-driven self-assembly: From discrete cages to infinite polycatenanes step by step. *Chemical Communications*, **49** (7).
7. El-Sayed, E.S.M., and Yuan, D. (2020) Metal-organic cages (MOCs): From Discrete to Cage-based Extended Architectures. *Chem Lett*, **49** (1), 28–53.
8. Shen, Y., Zhu, H. Bin, Hu, J., and Zhao, Y. (2015) Construction of a metal-organic framework by octuple intercatenation of discrete icosahedral coordination cages. *CrystEngComm*, **17** (10).
9. Kuang, X., Wu, X., Yu, R., Donahue, J.P., Huang, J., and Lu, C.Z. (2010) Assembly of a metal-organic framework by sextuple intercatenation of discrete adamantane-like cages. *Nat Chem*, **2** (6), 461–465.
10. Jiang, L., Ju, P., Meng, X.R., Kuang, X.J., and Lu, T.B. (2012) Constructions of two polycatenanes and one polypseudo-rotaxane by discrete tetrahedral cages and stool-like building units. *Sci Rep*, **2**.

11. Patat, F., and Derst, P. (1959) On the thermal degradation of polymeric phosphonitrile chloride. *Angewandte Chemie*, **71** (3).

12. Fujita, M., and Ogura, K. (1996) Transition-metal-directed assembly of well-defined organic architectures possessing large voids: From macrocycles to [2]catenanes. *Coord Chem Rev*, **148**, 249–264.

13. Yu, W., Qiu, F.Y., Luo, S.T., Shi, H.T., Yuan, G., and Wei, X. (2021) Coordination assembly and host-guest chemistry of a triply interlocked [2]catenane. *Inorg Chem Front*, **8** (9), 2356–2364.

14. Chimica, I. (2021) Exploring the solid-state synthesis and host-guest chemistry of M12L8 poly- [n] -catenanes using the tris-pyridyl benzene ligand.

15. Omar K Farha 1, A Özgür Yazaydın, Ibrahim Eryazici, Christos D Malliakas, Brad G Hauser, Mercouri G Kanatzidis, SonBinh T Nguyen, Randall Q Snurr, J.T.H. De novo synthesis of a metal-organic framework material featuring ultrahigh surface area and gas storage capacities.

16. Leslie J. Murray, a M.D.J.R.L. Hydrogen storage in metal–organic frameworks†.

17. Myunghyun Paik Suh 1, Hye Jeong Park, Thazhe Kootteri Prasad, D.-W.L. Hydrogen storage in metal-organic frameworks.

18. Sun, Z., Li, P., Xu, S., Li, Z.Y., Nomura, Y., Li, Z., Liu, X., and Zhang, S. (2020) Controlled Hierarchical Self-Assembly of Catenated Cages. *J Am Chem Soc*, **142** (24), 10833–10840.

19. Fujita, M., and Ogura, K. (1996) Supramolecular Self-Assembly of Macrocycles, Catenanes, and Cages through Coordination of Pyridine-Based Ligands to Transition Metals. *Bull Chem Soc Jpn*, **69** (6).

20. Martí-Rujas, J., and Kawano, M. (2013) Kinetic products in coordination networks: Ab initio X-ray powder diffraction analysis. *Acc Chem Res*, **46** (2), 493–505.

21. Liu, G., Rauscher, P.M., Rawe, B.W., Tranquilli, M.M., and Rowan, S.J. (2022) Polycatenanes: synthesis, characterization, and physical understanding. *Chem Soc Rev*, **51** (12), 4928–4948.

22. Fischer, J., Lang, M., and Sommer, J.U. (2015) The formation and structure of Olympic gels. *Journal of Chemical Physics*, **143** (24).

23. Yang, C., and Chen, H. (2022) A Roadmap for Mechanically Interlocked Molecular Junctions at Nanoscale. *ACS Appl Nano Mater*, **5** (10).

24. Raee, E., Yang, Y., and Liu, T. (2021) Supramolecular structures based on metal-organic cages. *Giant*, **5**, 1–19.

25. Fujita, M. (1999) Self-assembly of [2]catenanes containing metals in their backbones. *Acc Chem Res*, **32** (1).

26. Fujita, M., Fujita, N., Ogura, K., and Yamaguchi, K. (1999) Spontaneous assembly of ten components into two interlocked, identical coordination cages. *Nature*, **400** (6739).

27. Ohmori, O., Kawano, M., and Fujita, M. (2005) Construction of biporous coordination networks viaπâ€" π interaction. *CrystEngComm*, **7**, 255–259.

28. Ohmori, O., Kawano, M., and Fujita, M. (2005) A two-in-one crystal: Uptake of two different guests into two distinct channels of a biporous coordination network. *Angewandte Chemie - International Edition*, **44** (13), 1962–1964.

29. Ohmori, O., Kawano, M., and Fujita, M. (2004) Crystal-to-crystal guest exchange of large organic molecules within a 3D coordination network. *J Am Chem Soc*, **126** (50), 16292–16293.

30. Fujita, M., Tominaga, M., Hori, A., and Therrien, B. (2005) Coordination assemblies from a Pd(II)-cornered square complex. *Acc Chem Res*, **38** (4).

31. Kawamichi, T., Kodama, T., Kawano, M., and Fujita, M. (2008) Single-crystalline molecular flasks: Chemical transformation with bulky reagents in the pores of porous coordination networks. *Angewandte Chemie - International Edition*, **47** (42), 8030–8032.

32. Heine, J., Schmedt Auf Der Günne, J., and Dehnen, S. (2011) Formation of a strandlike polycatenane of icosahedral cages for reversible one-dimensional encapsulation of guests. *J Am Chem Soc*, **133** (26).

33. Beheshti, A., Nozarian, K., Mousavifard, E.S., Abrahams, C.T., Mayer, P., Gajda, R., Woźniak, K., and Motamedi, H. (2021) Design and construction of the imidazole-2-thione-based copper(I) complexes by varying the co-anion and synthesis conditions and verifying their antimicrobial activity. *J Solid State Chem*, **294**.

34. Giordana, A., Priola, E., Gariglio, G., Bonometti, E., Operti, L., and Diana, E. (2021) Reticular chemistry applied on coordination polymers of Copper(I) cyanide with tridentate ligands: effect of the ligand flexibility and donor properties on topology, dimensionality and reaction behavior in solvothermal conditions. *Polyhedron*, **198**.

35. Kang, J., Lee, Y., Kim, S., Yun, H., and Do, J. (2014) 1D and 2D cobalt(II) coordination polymers, Co(ox)(en): Synthesis, structures and magnetic properties. *Bull Korean Chem Soc*, **35** (11).

36. Damjanović, V., Pisk, J., Kuzman, D., Agustin, D., Vrdoljak, V., Stilinović, V., and Cindrić, M. (2019) The synthesis, structure and catalytic properties of the [Mo<inf>7</inf>O<inf>24</inf>(μ-Mo<inf>8</inf>O<inf>26</inf>)Mo<inf>7</inf>O<inf>24</inf>]$^{16-}$ anion formed: Via two intermediate heptamolybdates [Co(en)<inf>3</inf>]<inf>2</inf>[NaMo<inf>. *Dalton Transactions*, **48** (27).

37. Romero, I., Rodríguez, M., Llobet, A., Corbella, M., Fernández, G., and Collomb, M.N. (2005) EPR and magnetic properties of [Mn(μ-Cl)2(bpy)]n: An unusual ferromagnetic interaction in a Mn(II) chloro-bridged polymer. *Inorganica Chim Acta*, **358** (15).

38. Tahli, A., MacLaren, J.K., Boldog, I., and Janiak, C. (2011) Synthesis and crystal structure determination of 0D-, 1D- and 3D-metal compounds of 4-(pyrid-4-yl)-1,2,4-triazole with zinc(II) and cadmium(II). *Inorganica Chim Acta*, **374** (1).

39. Gu, Z.M., Wang, Q.L., Niu, Y.Y., Guo, X.L., Hou, H.W., Fan, Y.T., and Sun, D. (2011) 2D d10 metal assembly frameworks: Construction of metal-organic architecture with metal thiocyanate and dipyridyl spacer. *J Chem Crystallogr*, **41** (4).

40. Pilgrim, B.S., and Champness, N.R. (2020) Metal-Organic Frameworks and Metal-Organic Cages – A Perspective. *Chempluschem*, **85** (8), 1842–1856.

41. J. Marti-Rujas (2023) Connecting metal-organic cages (MOCs) for CO2 remediation. *Mater. Adv.*

42. Sun, Q.F., Iwasa, J., Ogawa, D., Ishido, Y., Sato, S., Ozeki, T., Sei, Y., Yamaguchi, K., and Fujita, M. (2010) Self-assembled M24L48 polyhedra and their sharp structural switch upon subtle liqand variation. *Science (1979)*, **328** (5982).

43. Wang, D., Zhang, Y., Gao, J., Ge, G., and Li, C. (2019) A Polyhedron-Based Heterometallic MOF Constructed by HSAB Theory and SBB Strategy: Synthesis, Structure, and Adsorption Properties. *Cryst Growth Des*, **19** (8).

44. Torresi, S., Famulari, A., Martí-Rujas, J., and Martí-Rujas, J. (2020) Kinetically Controlled Fast Crystallization of M12L8Poly-[n]-catenanes Using the 2,4,6-Tris(4-pyridyl)benzene Ligand and ZnCl2in an Aromatic Environment. *J Am Chem Soc*, **142** (20), 9537–9543.

45. Haneda, T., Kawano, M., Kawamichi, T., and Fujita, M. (2008) Direct observation of the labile imine formation through single-crystal-to-single-crystal reactions in the pores of a porous coordination network. *J Am Chem Soc*, **130** (5), 1578–1579.

46. Kitagawa, S., Kitaura, R., and Noro, S.I. (2004) Functional porous coordination polymers. *Angewandte Chemie - International Edition*, **43** (18).

47. Martí-Rujas, J., Islam, N., Hashizume, D., Izumi, F., Fujita, M., and Kawano, M. (2011) Dramatic structural rearrangements in porous coordination networks. *J Am Chem Soc*, **133** (15), 5853–5860.

48. Martí-Rujas, J., Islam, N., Hashizume, D., Izumi, F., Fujita, M., Song, H.J., Choi, H.C., and Kawano, M. (2011) Ab initio powder diffraction structure analysis of a host-guest network: Short contacts between tetrathiafulvalene molecules in a pore. *Angewandte Chemie - International Edition*, **50** (27), 6105–6108.

49. Rosen, B.M., Huang, C., and Percec, V. (2008) Sequential Ni-catalyzed borylation and cross-coupling of aryl halides via in situ prepared neopentylglycolborane. *Org Lett*, **10** (12).

50. Tashiro, S., Kubota, R., and Shionoya, M. (2012) Metal-macrocycle framework (MMF): Supramolecular nano-channel surfaces with shape sorting capability. *J Am Chem Soc*, **134** (5), 2461–2464.

51. D. Blakemore, "Chapter 1:Suzuki–Miyaura Coupling," RSC Drug Discovery Series, Vols. 2016-January, no. 52, pp. 1-69, 5 2016.

52. Martí-Rujas, J., Elli, S., and Famulari, A. (2023) Kinetic trapping of 2,4,6-tris(4-pyridyl)benzene and ZnI2 into M12L8 poly-[n]-catenanes using solution and solid-state processes. *Sci Rep*, **13** (1).

Appendix: supporting information

For what concern the first chapter in **Results and Discussion**, some crystallographic changes in the lattice has been declared in the section. However, these modifications have not been included in the section in order to maintain the readability of the text. Henceforth, supplementary material is shown below.

Along with pX, also mX and oX single crystals are synthesized through *three-layer method*. Conversely to pX, however, the other isomers preferentially form Coordination polymers instead of Catenanes (slow crystallization let the thermodynamic product to form: it means pX is stable in a catenane framework, whilst mX is stabler in a less organized CP). A computational representation and lattice parameters are provided below.

	a / α	**b / β**	**c / γ**	**Volume**
Length [A]	31.85	12.76	17.27	6951
Angle [°]	90	97.74	120	

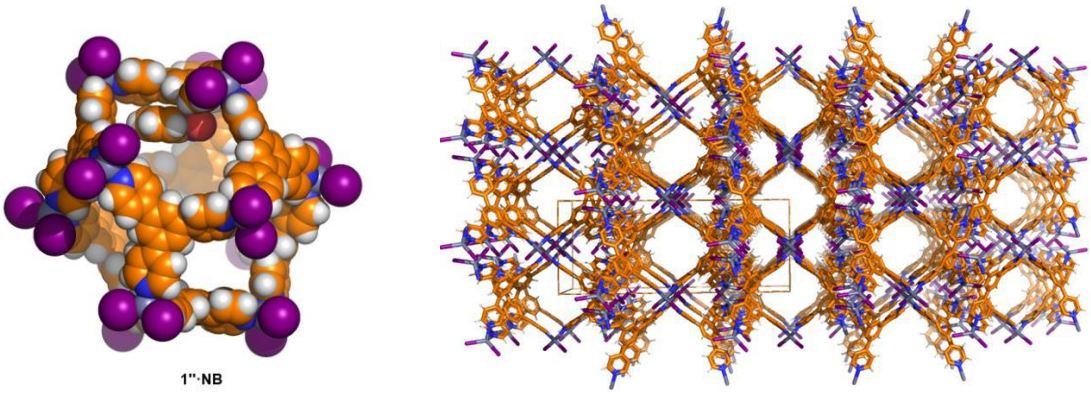

Figure 18 *Representation of a icosahedral nanocage and a CP framework.*

A single crystal of $\mathbf{M_{12}L_8(pX)_{12}}$ is let grow up and then undergoes multiple SCSC (in the ascending order). Lattice parameters are the following:

length [Å]	a	b	c	Volume
$M_{12}L_8(pX)_{12}$	38.86	38.86	16.24	21235
$M_{12}L_8(o\text{-}DCB)_6$	38.37	38.37	15.59	19884
$M_{12}L_8(NB)_6$	38.64	38.64	16.09	20813
$M_{12}L_8(pX)_6$	38.83	38.83	16.00	20896
$M_{12}L_8(NB)_6$	38.77	38.77	15.99	20817

Table 2 *Lattice parameters about consecutive SCSC processes onto the same $M_{12}L_8G_x$ single crystal*

List of Figures

List if Tables

List of symbols

Acronym	Description
MOF	Metal-Organic Cage
MIM	Mechanically-Interlocked Molecule
CP/CN	Coordination Polymer/Network
MOC	Metal-Organic Cage
TPB	2,4,6-tris-(4-pyridyl)benzene
***p*X**	paraxylene
***o*-DCB**	ortodichlorobenzene
NB	nitrobenzene
EB	ethylbenzene
GI/GE	Guest inclusion/exchange